Lu *et al. Biochar* (2022) 4:45
https://doi.org/10.1007/s42773-022-00173-y

Biochar

REVIEW Open Access

Application of biochar-based photocatalysts for adsorption-(photo)degradation/reduction of environmental contaminants: mechanism, challenges and perspective

Yin Lu[1*], Yawen Cai[2], Sai Zhang[3], Li Zhuang[2], Baowei Hu[2], Suhua Wang[4], Jianrong Chen[5] and Xiangke Wang[2,3*]

Abstract

The fast increase of population results in the quick development of industry and agriculture. Large amounts of contaminants such as metal ions and organic contaminants are released into the natural environment, posing a risk to human health and causing environment ecosystem problems. The efficient elimination of contaminants from aqueous solutions, photocatalytic degradation of organic pollutants or the in-situ solidification/immobilization of heavy metal ions in solid phases are the most suitable strategies to decontaminate the pollution. Biochar and biochar-based composites have attracted multidisciplinary interests especially in environmental pollution management because of their porous structures, large amounts of functional groups, high adsorption capacities and photocatalysis performance. In this review, the application of biochar and biochar-based composites as adsorbents and/or catalysts for the adsorption of different contaminants, adsorption-photodegradation of organic pollutants, and adsorption-(photo) reduction of metal ions are summarized, and the mechanism was discussed from advanced spectroscopy analysis and DFT calculation in detail. The doping of metal or metal oxides is the main strategy to narrow the band gap, to increase the generation and separation of photogenerated e^{-}-h^{+} pairs, to produce more superoxide radicals ($\cdot O_2^-$) and hydroxyl radicals (·OH), to enhance the visible light absorption and to increase photocatalysis performance, which dominate the photocatalytic degradation of organic pollutants and (photo)reduction of high valent metals to low valent metals. The biochar-based composites are environmentally friendly materials, which are promising candidates in environmental pollution cleanup. The challenge and perspective for biochar-based catalysts are provided in the end.

Highlights

1. Adsorption-photocatalytic degradation of organic pollutants by biochar-based catalysts is summarized.
2. Adsorption-(photo)catalytic reduction-solidification of heavy metal ions is discussed.
3. Mechanism and active free radicals on the degradation/reduction of contaminants are compared and described.

*Correspondence: luyin@zjsru.edu.cn; xkwang@ncepu.edu.cn

[1] Key Laboratory of Pollution Exposure and Health Intervention of Zhejiang Province, College of Biological and Environment Engineering, Zhejiang Shuren University, Hangzhou 310015, People's Republic of China
[2] School of Life Science, Shaoxing University, Shaoxing 312000, People's Republic of China
Full list of author information is available at the end of the article

4. The methods to improve the photocatalysis performance of biochar-based catalysts are introduced.
5. The challenges for the real application of biochar-based materials are provided.

Keywords: Biochar-based composites, Adsorption, Photocatalytic degradation, Photocatalytic reduction, Environmental pollutants

Graphical Abstract

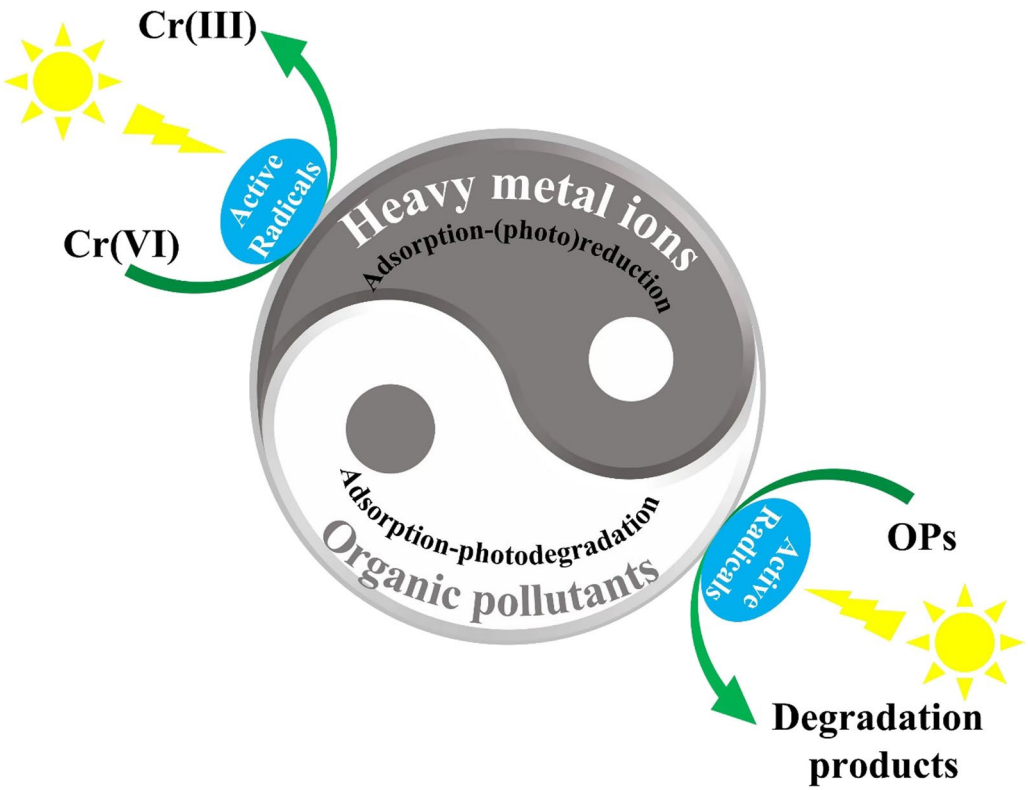

1 Introduction

With the quick growth and development of agriculture and industry, the life quality has been improved and thereby requires higher standard level of environmental ecosystem and daily supply. However, large amounts of various pollutants such as metal ions, persistent organic pollutants (POPs), antibiotic, cosmetics and dyes etc. are inevitably released into the natural environment such as soils, water, rivers, lakes etc. (Li et al. 2021a; Liu et al. 2021a, b; Zhang et al. 2021a). The pollutants in soils, lakes, rivers and groundwater etc. could be accumulated and at last enter into human body through food chain. Thereby, the efficient elimination of the pollutants from aqueous solutions is crucial for environmental protection and human health. Although different kinds of techniques such as (co)precipitation, membrane, adsorption, oxidation–reduction, degradation, ion exchange, transformation etc. have been applied to remove the pollutants from large volume of solutions or in-situ solidification/immobilization on solid phases (Chen et al. 2022a; Hao et al. 2021; Wang et al. 2022; Yu et al. 2021a, 2022), it is still a worldwide challenge for the efficient decontamination of pollutants from solid phases such as soils, sediments etc., especial at low concentrations (Liu et al. 2022a). The photocatalytic degradation of POPs or reduction of metal ions is one effective strategy for the in-situ decontamination, to reduce the organic contaminant concentration or immobilize the heavy metal ions on solid particles (Cai et al. 2022a; Cheng et al. 2021; Li et al. 2021b; Yang et al. 2021a; Zhang et al. 2022a).

Biochar is a kind of low cost and environmentally friendly material with high efficiency and facile production. It has attracted increase attention in wastewater treatment. The high surface areas, high porosities,

enough functional surface groups, excellent ion exchange ability and high stability make biochar a suitable material for pollution management. More importantly, the cooperation of biochar with other kinds of metals or metal oxides could enhance the adsorption capacity, increase visible light absorption and separation of photogenerated electrons and holes, reduce the band gap and thereby enhance the photocatalytic performance of biochar-based catalysts. The application of biochar and biochar-based materials has been extensively investigated in the decontamination of environmental pollutants.

Sutar et al. (2022) summarized the recent works about the application of biochar for the adsorption of textile dyes from wastewater, and also described the photocatalytic degradation of dyes using modified biochar simply. The biochar could remove dyes efficiently from aqueous solutions. However, the mechanism for the photocatalytic degradation of dyes was not described in detail, especially the relationship between the structures of catalysts and the degradation abilities for dyes, and the theoretical calculation/simulation of organic dye degradation mechanism and processes. Chandra et al. (2021) reviewed the preparation of TiO_2/biochar photocatalysts and their application in the photodegradation of sulfamethoxazole. The possible mechanism for the enhanced photocatalytic capacity of the composites was discussed. The ·OH free radical was the main active species for sulfamethoxazole degradation and the increase of the composite photocatalytic ability was ascribed to the photocatalytic response in UV–visible range (200–700 nm) and enhanced adsorption of sulfamethoxazole on the TiO_2/biochar composites. Gasim et al. (2022) summarized the methods for the functionality of biochar active sites and the application of the biochar for the removal of organic pollutants (OPs). The oxygen-containing functional groups, hybridized carbon and heteroatoms such S, N, P etc. could promote the organic molecule adsorption on the functionalized biochar through H-bonding, π–π interactions, ion exchange, and Coulombic attraction etc. The decontamination of OPs by the functionalized biochar could be achieved through physical adsorption, chemical interaction and redox reactions. The $\cdot O_2^-$, ·OH, and $^1O_2$ free active species generated in the advanced oxidation processes, and the $SO_4^{\cdot -}$ species produced by the activation of PS such as peroxydisulfate (PDS) and peroxymonosulfate (PMS), could degrade the OPs efficiently. The –OH or –NH groups could serve as H-donors, whereas the N or O atoms in benzene rings could serve as H-acceptors. The surface –OH or –COOH groups could promote the hydrophobic reaction with the hydrophobic organic molecules. The graphitic N in biochar can improve the photodegradation of OPs (Sun et al. 2019). Zhao et al. (2021) reviewed the modification of biochar with nanometal oxides to improve the surface area and to increase functional groups. The effects of experimental conditions (i.e., solution pH, temperature, ionic strength, etc.) on the removal of environmental contaminants to nanometal oxide modified biochar were compared, and the removal mechanism of pollutants was summarized. Surface precipitation, ion exchange, electrostatic interaction, H-bonding, π–π interactions etc. are the main mechanisms for the adsorption of organic or inorganic pollutants. Feng et al. (2021) summarized the synthesis of magnetic biochar through impregnation pyrolysis, chemical coprecipitation, reductive coprecipitation, solvothermal, oxidative hydrolysis, ball milling, cross-linking, physical mixing, and combined methods. The degradation of OPs using the different magnetic biochar was reviewed in PDS, PMS, Fenton-like, $NaBH_4$, and photocatalysis conditions. The relative contribution of different sections and active species in the magnetic biochar in the degradation of OPs were discussed and the authors concluded that the graphite structure, doped metals or supported metal oxides, oxygen-containing functional groups, and persistent free radicals had catalytic properties and promoted the reactive species to improve the OPs degradation. Li et al. (2020) summarized the preparation of magnetic biochar through coprecipitation, calcination and pyrolysis, and compared the advantages and disadvantages of the three methods, i.e., (1) coprecipitation produces the products with high purity in short time and simple reaction conditions; (2) calcination is simple to prepare magnetic biochar; and (3) pyrolysis method requires heavy mechanical system and inert gas to produce magnetic biochar. The adsorption of metal ions and POPs by magnetic biochar was reviewed and the adsorption mechanism varied with pollutants and was influenced by the functional surface groups, pore structures and chemical bonds on magnetic biochar surfaces. The authors gave the perspective that the photocatalytic degradation of organic contaminants by magnetic biochar-based catalysts may be the research hotspot in future. Minh et al. (2020) summarized the synthesis and functionalization of biochar and the application as catalysts for the degradation and mineralization of emerging OPs. The functional active moieties, free active radicals, charge transfer, hierarchical porosity, graphitic degree and redox potential on the degradation of OPs were evaluated and discussed in detail. The high photocatalytic, electrocatalytic and chemo-catalytic properties are attributed to the excellent chemical and electrical configuration of biochar.

The application of biochar for the remediation of organic contaminants showed that the adsorption properties were related to the pyrolyzing temperature (Zhang et al. 2020). Zheng et al. (2019) modified biochar with g-C_3N_4 containing N-functional groups,

which showed better thermal stability than pristine biochar. The composites showed good adsorption ability and photocatalytic degradation activity to reactive red 120 dye. Lu et al. (2020) summarized the synthesis of magnetic biochar, 2D biochar-based membrane, and 3D macrostructure biochar, and the relationship between the adsorption abilities and structural properties. The relationship between adsorption, catalysis and redox properties and structure of biochar is discussed, pointing out that structure-functionalization-reactivity is important for understanding the interaction mechanism of pollutants with biochar, which is also crucial for the synthesis and application of biochar. Our research group summarized the recent works about the synthesis of biochar and biochar-based materials and their application in the removal of organic and inorganic pollutants from aqueous solutions and immobilization in soils (Huang et al. 2019; Liang et al. 2021; Qiu et al. 2022). The preferential interactions of organic molecules with biochar were mainly attributed to π-π interactions, hydrophobic effect and H-bonding, whereas the adsorption of metal ions was mainly dominated by ion exchange, surface complexation, (co) precipitation and adsorption-reduction on biochar. The adsorption mechanism was discussed from batch results and spectroscopy analysis. However, the photocatalytic degradation/reduction of contaminants was not discussed in detail, especially the contribution of different free active species on the degradation/reduction of contaminants. The theoretical calculations of pollutant molecule with biochar were simulated using density functional theory (DFT) and molecular dynamics (MD) (Hu et al. 2020). To our best knowledge, this is the first paper to discuss the computational calculation of pollutants' interaction with biochar although the authors simplified the structure of biochar. The authors gave the reason for the complicated structures, which is impossible to carry out DFT or MD simulation exactly. The computational model of biochar was based on the aromatic carbon ring cluster model because biochar is composed of carbonaceous skeleton and functional groups. Till now, no DFT or MD calculation about the photocatalytic degradation or interaction of pollutants with real biochar or biochar-based materials was available. Qiu et al. (2021) summarized the main challenges and main problems for the application of biochar-based composites as photocatalysts for the photocatalytic degradation of OPs, and considered that the photocatalytic process is still "black-box", the intermediate products' real-time on-line analysis, efficient photogeneration and separation of e^{-}-h^{+} pairs, effective visible light absorption and control of final products are the main challenges in future. They pointed out that no computational simulation of organic photocatalytic degradation is available, which may be attributed to the unclear complicated structures of biochar.

From the abovementioned references, one can see that biochar has been extensively studied for the removal of OPs and heavy metal ions. The adsorption mechanism has been discussed in detail. The photocatalytic degradation of OPs is an effective method to decontaminate OPs using biochar-based catalysts, and the relative contribution of photogenerated active species on the photocatalytic degradation of OPs can be evaluated from quenching and ESR tests. However, the relationship between the structures of biochar-based catalysts and photocatalytic ability, the contribution of relevant components in the catalyst to photocatalytic performance, especially the photocatalytic reduction-solidification of heavy metal ions and the mechanism discussion from advanced spectroscopic analysis and computational calculation are still scarce. As the preparation of biochar and biochar-based composites has been mentioned in detail in the aforementioned references, we did not describe the methods and techniques for the preparation of biochar and biochar-based composites in this review. Herein we mainly summarized and discussed the newly recent works about the application of biochar-based photocatalysts in the adsorption-photocatalytic degradation of OPs and adsorption-(photo)catalytic reduction-solidification of heavy metal ions, especially in last 5 years. The removal of OPs and heavy metal ions through adsorption technique is not described in detail in this review. The contribution of metals or metal oxides to the photocatalytic properties of biochar-based catalysts, and the contribution of free active radicals to the photo-degradation/reduction of pollutants are mainly reviewed and compared, and the mechanisms are discussed in this review. The challenge and perspective in future are described in conclusion section.

2 Heavy metal ions

The elimination of heavy metal ions from aqueous solutions using different techniques such as ion exchange, adsorption, (co)precipitation, membrane separation, biology preconcentration, electrocatalytic/photocatalytic reduction-precipitation, and oxidation–reduction etc. has been extensively studied (Cai et al. 2022b; Hao et al. 2022a; Wang et al. 2019a). Herein, we mainly summarized the recent works for the elimination/immobilization of metal ions using the adsorption-photocatalytic/electrocatalytic reduction strategy. In this section, we separately summarized the recent works for metal anions and cations.

2.1 Metal anions

2.1.1 Zn-based biochar

Cr(VI) is the main metal anion in the natural environment and has been studied extensively because of its high toxicity and mobility. Yu et al. (2018) prepared ZnO-biochar composites and applied them for the removal of Cr(VI). 95% Cr(VI) removal was achieved with 30% ZnO-loaded biochar and precipitation of $Cr(OH)_3$ on ZnO occurred as ZnO generated electrons to reduce Cr(VI) to Cr(III) under light irradiation. Yu et al. (2020) synthesized biochar from corn stalks and modified it with $FeCl_3$ and $ZnCl_2$. The modified biochar showed an adsorption capacity of 139 mg/g for Cr(VI) at pH 2, which was mainly attributed to electrostatic interaction of the negatively charged Cr(VI) to the positively charged surface of biochar. The B-H group and $ZnFe_2O_4$ in biochar could provide electrons for the photoreduction of Cr(VI) and formed $ZnFeCrO_4$ and $FeCr_2O_4$ precipitates on biochar. Zn-based biochar could efficiently eliminate Cr(VI) from aqueous solutions, and formed precipitates on solid particles.

2.1.2 Bi-based biochar

Geng et al. (2020) prepared BiOBr/biochar composites for the photoreduction of Cr(VI). The BiOBr could enhance the generation and separation of photogenerated e^--h^+ pairs. The photogenerated electrons (e^-) could reduce Cr(VI) to Cr(III) through a reduction process and the BiOBr provided more active sites for the photoreduction of Cr(VI). Wang et al. (2020) synthesized Bi_2WO_6-loaded N-doped biochar (BW/N-B) and applied it for the removal and photoreduction of Cr(VI) from wastewater. The band gap of BW/N-B was narrowed from 2.52 eV to 2.28 eV (value of Bi_2WO_6), which facilitated the separation and migration of photogenerated e^--h^+ pairs and thereby enhanced the photocatalytic property. 30% Cr(VI) was adsorbed by the composites while 97% Cr(VI) was reduced to Cr(III) in 30 min under visible light irradiation, suggesting the high efficient elimination and solidification of Cr(VI) on the composites. The BiOBr/biochar catalyst showed high photocatalysis performance in the removal of inorganic and organic pollutants in wastewater treatment.

Mao et al. (2021) synthesized S, N-codoped Bi_2WO_6/biochar for the removal of Cr(VI) from solutions, and found that 99% Cr(VI) (10 mg/L) was removed in 75 min with high selectivity in the presence of coexisting ions such as Cl^-, SO_4^{2-}, Ca^{2+} and CO_3^{2-} in wide pH range (3–9) under visible light irradiation. The narrow band gap favors the visible light absorption and photogenerated electron transfer, which promotes the photocatalytic performance. The generated $\cdot O_2^-$, ·OH, O_2 could reduce Cr(VI) to Cr(III) (Fig. 1a). However, the function of the doped N and S atoms in the photocatalytic reduction was not described and discussed in detail. The contribution of codoped N and S was not studied and still unclear. The doping of metal and nonmetal ions could change band gap, increase the light absorption, efficiently separate the electron–hole pairs etc., thereby enhancing the photocatalysis performance of the catalysts.

2.1.3 Fe-based biochar

Mandal et al. (2017) incorporated chitosan and zero valent iron (ZVI) to biochar and applied it to immobilize Cr(VI) in soil. The functional oxygen-containing groups such as carboxyl, phenolic and carbonyl acted as proton donors for Cr(VI) reduction to Cr(III). The amine groups of chitosan could bind Cr(VI) strongly and ZVI could reduce Cr(VI) to Cr(III) efficiently. The addition of chitosan and ZVI-modified biochar to soil could reduce Cr(VI) to Cr(III) obviously and then adsorbed on biochar or immobilized in soil through strong surface complexation and precipitation reactions (Fig. 1b). Liang et al. (2019) synthesized magnetic biochar for the removal of Cr(VI) from wastewater and achieved an adsorption capacity of 55 mg/g. The biochar provided active sites for Cr(VI) binding and electron-donor groups for Cr(VI) reduction to Cr(III), whereas Fe_3O_4 immobilized the reduced Cr(III) to form Cr(III)-Fe(III) hydroxides. Cho et al. (2017) prepared magnetic biochar from spent coffee ground and applied it for the removal of As(V) from wastewater. The Fe_3C and Fe_3O_4 phases in the composites contributed to the uptake of As(V) rather than the porosity and functional groups of biochar. However, it is well known that As(III) is more toxicity than As(V) in the natural environment. Dong et al. (2014) applied biochar for the reduction of Cr(VI) and oxidation of As(III) in the presence of organic matter, and found that the dissolved organic matter (DOM) could enhance As(III) oxidation and Cr(VI) reduction. More importantly, the reduction of Cr(VI) was coupled with the oxidation of As(III) in the absence of DOM. The adsorption of As(III) by biochar-based materials is still rarely explored and the interaction mechanism especially the structure information of As(III)/As(V) such as bonding coordination with different groups or atoms has not been intensively studied. Fan et al. (2020) synthesized nZVI-based biochar and applied it for the immobilization of As(V) in soil. The results showed that the adsorbed As(V) was reduced to As(III) by nZVI, which could immobilize As(III) on biochar efficiently. Tan et al. (2019) applied ZVI-based biochar for the removal of Se(IV) and Se(VI) from solutions, and achieved an adsorption capacity of 62.5 mg/g for Se(IV) and 35.4 mg/g for Se(VI), which was mainly due to the ZVI and positive surface charge of the composites.

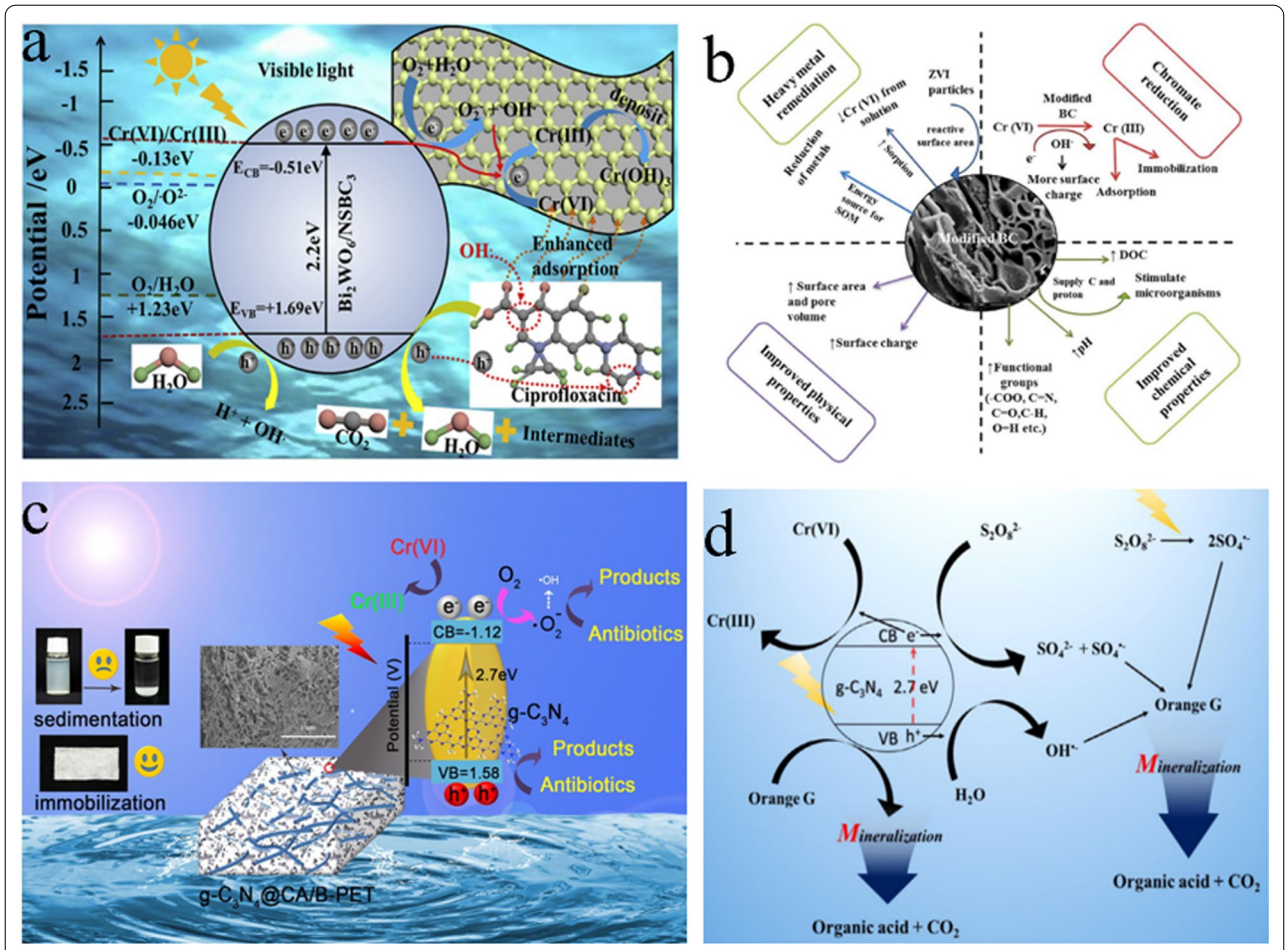

Fig. 1 Photocatalytic degradation of CIP and reduction of Cr(VI) by S,N-codoped Bi_2WO_6/biochar (**a**) (Mao et al. 2021); Possible mechanism of Cr(VI) interaction with biochar and photoreduction (**b**) (Mandal et al. 2017); Photocatalytic degradation of Cr(VI) by C_3N_4@CA/B-PET (**c**) (Chen et al. 2019a); Photooxidation and reduction of organic pollutants and Cr(VI) under UV light (**d**) (Jeon et al. 2017)

Se(VI)/Se(IV) were reduced to Se(− II)/Se(0), which were less toxicity and solubility. The presence of other metal ions such as Ca^{2+}, K^+ and Mg^{2+} could enhance the removal of Se(VI)/(Se(IV) slightly, indicating the efficient elimination of Se(VI)/Se(IV) from complicated systems.

2.1.4 C_3N_4-based biochar

Chen et al. (2019a) synthesized C_3N_4@CA/B-PET and applied it for the photoreduction of Cr(VI) from wastewater. The hexavalent Cr(VI) could be reduced to trivalent Cr(III) in the coexisting sulfaquinoxaline sodium under sunlight irradiation. The composites could simultaneously eliminate Cr(VI) and antibiotics with high stability and reusability (Fig. 1c). Jeon et al. (2017) prepared biochar/C_3N_4 composites and applied them for the removal of Cr(VI) and Orange G from aqueous solutions. Orange G was oxidized and mineralized to form organic acid and CO_2, whereas Cr(VI) was photo-reduced to Cr(III) under UV light conditions. The addition of persulfate enhanced the oxidation rate, which was attributed to the effective activation of persulfate to sulfate radicals by biochar. The schematic diagram of Cr(VI) reduction and Orange G oxidation under UV light irradiation is shown in Fig. 1d. Li et al. (2019a) synthesized biochar-coupled C_3N_4 nanosheets (biochar-C_3N_4) and applied them for the removal of Cr(VI) from wastewater by adsorption combined with photoreduction strategy. The surface adsorbed Cr(VI) was reduced by photogenerated e^- species and then stabilized on biochar-C_3N_4 composites. The Cr(VI) was firstly adsorbed on the composites, and the photogenerated electrons generated by C_3N_4 were transferred to the composites. Then the adsorbed Cr(VI) was reduced to Cr(III) and stably fixed by electrostatic interaction with the C-H surface groups. The detailed process and the possible reactions for the reduction of Cr(VI) to Cr(III) are shown in Fig. 2. Rajapaksha et al. (2018) found that the adsorption of Cr(VI) on biochar was high at low

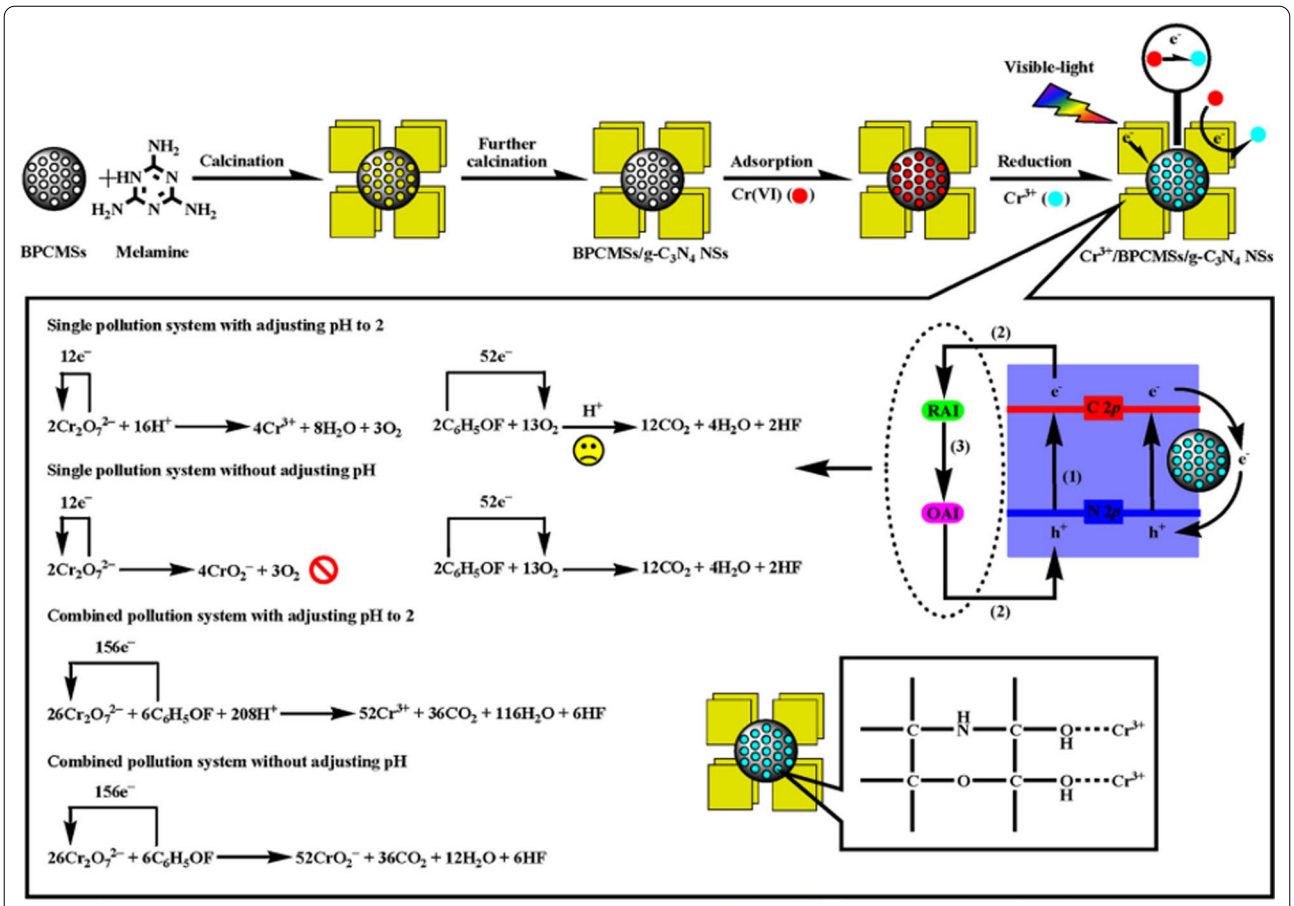

Fig. 2 Fabrication of biochar-coupled C_3N_4 nanosheets and possible reactions for the reduction of Cr(VI) to Cr(III) under different experimental conditions (Li et al. 2019a)

pH values (2–5), and then decreased with the increase of pH, which was in good agreement with the surface charge of biochar and Cr(VI) species. The X-ray absorption fine structure (XAFS) analysis suggested the reduction of Cr(VI) to form $Cr(OH)_3$ precipitate.

2.1.5 Others

Zhao et al. (2018) prepared biochar from corn straw and applied it for the selective removal of Cr(VI) in the presence of high salts. Cr(VI) could be reduced to Cr(III) at pH ~ 7, which was different with most other studies that Cr(VI) was only reduced to Cr(III) at low pH values (i.e., pH = 2 ~ 4). The ESR and free radical quenching analysis indicated that the persistent free radicals on biochar played important roles in the reduction of Cr(VI) to Cr(III) by forming $Cr(OH)_3$. Zhang et al. (2018a) prepared biochar from tobacco petiole under different pyrolysis temperatures and applied it for the removal of Cr(VI) from solution. The results showed that the adsorption of Cr(VI) was affected by the surface functional groups rather than surface areas. The adsorption capacity increased with the increase of pyrolysis temperature, and the surface carboxyl groups could reduce Cr(VI) to Cr(III). Zhang et al. (2018b) applied biochar for the removal of Cr(VI) from aqueous solutions, and achieved 99.8% removal efficiency at pH = 3, dosage of 5 g/L and Cr(VI) initial concentration of 10 mg/L. The high removal was attributed to the adsorption-reduction-adsorption steps, i.e., Cr(VI) was adsorbed on biochar and then reduced to Cr(III), which was further adsorbed on biochar with an adsorption capacity of 25 mg/g. The main mechanisms for the photocatalytic reduction of Cr(VI) using different biochar-based catalysts are shown in Table 1. Zheng et al. (2021) summarized the synthesis and modification of different biochars. The advantages/disadvantages of different methods for the production of biochar were compared. The adsorption, electron shuttle, reduction and photoreduction of Cr(VI) by biochar under different conditions were reviewed, and the possible interaction mechanisms such as ion exchange, surface complexation, precipitation, electrostatic interaction, physisorption, chemisorption etc. were discussed

Table 1 Summary of biochar-based catalysts in the photocatalytic reduction of heavy metal ions

Catalysts	Pollutants	Mechanisms and main active radicals	References
ZnO-biochar	Cr(VI)	Formation of $Cr(OH)_3$ precipitation; photogenerated e^-	Yu et al. (2018)
MgO-biochar	Cr(VI)	Chemical adsorption of Cr(VI); Cr(VI) reduction to Cr(III) by electron-donor groups	Xiao et al. (2018)
BiOBr-biochar	Cr(VI)	Cr(VI) reduced to Cr(III) by photogenerated e^-	Geng et al. (2020)
S,N-codoped Bi_2WO_6-biochar	Cr(VI)	Photogenerated $\cdot O_2^-$, $\cdot OH$ reduced Cr(VI) to Cr(III)	Mao et al. (2021)
Chitosan/ZVI-biochar	Cr(VI)	Amine groups bind Cr(VI) and ZVI reduced Cr(VI) to Cr(III) to form precipitation	Mandal et al. (2017)
C_3N_4-biochar	Cr(VI)	Sulfate radicals formed by persulfate and reduced Cr(VI) to Cr(III)	Jeon et al. (2017)
Biochar	Cr(VI)	Cr(VI) reduction to Cr(III), evidenced by XAFS analysis. Electron-donor groups contributed Cr(VI) reduction to Cr(III)	Rajapaksha et al. (2018)
Fe_3O_4-biochar	Cr(VI)	Cr(VI) was reduced by electron-donor groups to form Cr(III)-Fe(III) hydroxides	Liang et al. (2019)
Bi_2WO_6-biochar	Cr(VI)	Photogenerated e^--h^+ pairs reduced Cr(VI) to Cr(III)	Wang et al. (2020)
$ZnFe_2O_4$-biochar	Cr(VI)	B-H group and $ZnFe_2O_4$ provided electrons for Cr(VI) photoreduction and formed $ZnFeCrO_4$ and $FeCr_2O_4$ precipitates	Yu et al. (2020)
Magnetic biochar	As(V)	Fe_3C and Fe_3O_4 contributed to As(V) uptake	Cho et al. (2017)

*It is necessary to note that although the names of some catalysts are the same, they are not the same materials

for different conditions, and the authors concluded that adsorption-reduction-adsorption and reduction-adsorption were the two mainly pathways for the immobilization of Cr(VI). Xiao et al. (2018) prepared MgO-coated biochar and applied it for the removal of Cr(VI) from solutions. The Cr(VI) ions were directly adsorbed by chemical interaction of Cr(VI) with MgO, and then reduced to Cr(III) by electron-donor groups.

From the abovementioned results, it is clear that the works about the adsorption-photoreduction elimination of heavy metal ions mainly focused on adsorption-photoreduction of Cr(VI) to Cr(III), and only few works focused on the adsorption-oxidation of As(III) to As(V), and Se(VI)/Se(IV) reduction to Se(0)/Se(− II). This is mainly attributed to the high toxicity of Cr(VI) and the possible photocatalytic reduction of Cr(VI) to Cr(III) by biochar-based catalysts under visible light irradiation. It is still relative difficult to achieve the photocatalytic reduction of Se(IV)/Se(VI) to Se(− II)/Se(0) under visible light irradiation.

2.2 Metal cations

As a kind of important nuclear fuel, uranium [U(VI)] also causes serious environmental pollution problems in nuclear energy utilization processes. The efficient extraction of U(VI) from wastewater or seawater is not only crucial to fission-based nuclear reactors, but also to environmental pollution management (Hao et al. 2022b). The photocatalytic reduction of U(VI) is an efficient method to extract or immobilize U(VI) from aqueous solutions. Chen et al. (2022b) summarized the recent works about the visible light-driven photocatalytic strategy for the selective U(VI) extraction, and concluded that the stability, the structure, surface functional groups, the band gap and visible light absorption properties of catalysts are crucial for U(VI) adsorption-photocatalytic reduction. Alam et al. (2018) studied the adsorption of U(VI) on biochar and found that the proton-active carboxyl group (–COOH) and phenolic hydroxy group (–OH) contributed mainly to U(VI) uptake, suggesting the importance of the functional groups on U(VI) adsorption.

2.2.1 Fe-based biochar

Chen et al. (2021a) synthesized chitosan-FeS@biochar and applied it for the removal of U(VI) from solutions. The result showed that chitosan could prevent FeS NPs aggregation and thereby enhanced the stability and reduction of U(VI) to U(IV). Liu et al. (2021c) applied SFeS@biochar for the adsorption of U(VI) and found that the removal of U(VI) was mainly dominated by electrostatic attraction, precipitation, surface complexation and reduction of U(VI) to U(IV), which was mainly attributed to iron sulfide nanoparticles. Pang et al. (2019) synthesized biochar supported sulfide NZVI and used it for U(VI) removal from solutions. The adsorption capacity achieved 428 mg/g at pH 5, and the spectroscopy analysis revealed the adsorption and reduction of U(VI) by sulfide NZVI. Hu et al. (2018) applied magnetic biochar for the removal of U(VI) from aqueous solution, and characterized the adsorbed materials using XPS and EXAFS techniques. The magnetic biochar could efficiently remove U(VI) from large volumes of aqueous solutions with good stability at pH = 3. The spectroscopy analysis showed the formation of U-Fe and U-U shells, suggesting the reduction and co-precipitation of U(VI) to U(IV). The adsorption of U(VI) by FeS@biochar showed that the presence of FeS significantly enhanced U(VI) removal and FeS could reduce U(VI) to U(IV) with high efficiency and

chemical stability (Chen et al. 2021b). Baig et al. (2014) applied magnetic biochar for the removal of As(III, V) from aqueous solutions, and achieved an adsorption capacity of 2.0 mg/g for As(III) and 3.1 mg/g for As(V). The magnetic biochar could efficiently remove As(III, V) from solutions although the presence of PO_4^{3-} inhibited the adsorption of As(III, V). The doping of iron or iron oxides could enhance the reduction ability and adsorption capacity of biochar, and thereby increase the elimination of metal ions from solutions.

2.2.2 Zn-based Biochar

Guo et al. (2022) synthesized 3D ZnO modified biochar and applied it for U(VI) removal. The adsorption capacity reached 239 mg/g at pH = 5 with high adsorption–desorption cycles and high stability. The mechanism was ion exchange with Zn^{2+} and complexation with –OH and –COOH surface groups. Yan et al. (2015) applied magnetic ZnS@biochar for Pb(II) removal from aqueous solutions, and achieved an adsorption capacity of 368 mg/g at pH = 6, much higher than other reported biochar materials. Li et al. (2018) prepared nano ZnO/ZnS modified biochar for the removal of Pb(II) and Cu(II) ions, which achieved an adsorption capacity of 136 mg/g for Pb(II) and 91 mg/g for Cu(II), much higher than the common biochar. The high adsorption of Pb(II) and Cu(II) was mainly attributed to the hydroxyl groups and the porous structures of Zn salt in the pyrolysis process. Xia et al. (2016) applied $ZnCl_2$-activated biochar for the removal of As(III) from solutions, and found that the hydroxyl groups in Zn-OH could form Zn–O–As(III) complexes. The adsorption could achieve equilibrium in 90 min with the adsorption capacity of 27.7 mg/g at pH = 7. Tho et al. (2021) applied ZnO modified biochar for the simultaneous removal of As(III), Pb(II) and Cd(II) from solutions, and achieved the adsorption tendency of Pb(II) > Cd(II) > As(III) at pH 6–7, with the adsorption capacities of 44.3 mg/g for Pb(II), 42.1 mg/g for Cd(II) and 39.5 mg/g for As(III). The cation exchange and surface precipitation are the main mechanisms for the adsorption of the metal ions. The modification of biochar with zinc salt could efficiently increase the adsorption capacity of biochar.

2.2.3 Others

Besides the abovementioned biochar composites, other kinds of biochar materials were also applied to extract metal cations from complicated systems. The adsorption-electrocatalytic strategy was applied to extract U(VI) from seawater using In-N single atom-doped carbon and achieved 6.35 mg/g in 24 h. The in-situ Raman, XPS and EXFA analysis showed that U(VI) could be electro-reduced to unstable U(V) intermediate, and then reduced to U(IV) and re-oxidized to U(VI) to form insoluble $Na_2O(UO_3{\cdot}H_2O)_x$ through the reversible single electron transfer on In-N sites (Liu et al. 2022b). Yang et al. (2021a) synthesized Fe–N-doped carbon for the selective extraction of U(VI) through adsorption-electroreduction technique from seawater, and the results showed that U(VI) could form $Na_2O(UO_3{\cdot}H_2O)_x$ precipitates, which could be easily collected from seawater. The material had good hydrophilicity with a water contact angle of 40 ° (Fig. 3a), which was helpful to improve the interaction of U(VI) on material surfaces. The adsorption capacity achieved ~ 90 mg/g in the spiked seawater at U(VI) initial concentration of 20 mg/g (Fig. 3b) with fast adsorption kinetics (150 min to achieve adsorption equilibrium, Fig. 3c). The XAFS analysis indicated the formation of $U(VI)O_2^{2+}$, and each U atom was coordinated with two axial O atoms, two O atoms from coordinated water molecules, two O atoms and N atoms from amidoxime groups (Fig. 3d and e). The cyclic voltammetry tests showed the sharp peak at − 0.77 V (vs SCE), suggesting the reduction of U(VI) to U(V), and the peak at − 0.43 V (vs SCE) suggested the oxidation of U(V) to U(VI) (Fig. 3f). The material showed the maximum adsorption capacity of 128 mg/g at 10 mg/g spiked seawater, suggesting the high extraction efficiency (Fig. 3g). More importantly, the yellow floc was formed on surface of carbon electrode, suggesting the U(VI) was transformed from seawater to electrode, forming precipitates and collecting on the electrode (Fig. 3h). From the results, one can see that the adsorption-electrocatalytic reduction of U(VI) is one of the most efficient methods to selective extraction of U(VI) from complicated systems. In near future, the co-doping the single metal ions on biochar for adsorption-electrocatalytic extraction of U(VI) or other kinds of heavy metal ions will attract extensively attraction.

The adsorption-reduction-solidification/precipitation of high valent metal ions to low valent metal ions is most efficient to immobilize the mobile metal ions in the natural environment, especially in soil, river or lake pollution treatment. It is really difficult to effectively extract the heavy metal ions from the complicated systems under natural conditions. The best method to reduce the toxicity and to prevent the transfer of heavy metal ions in the environment through food-chain is the in-situ solidification of metal ions in solid phases. The reduction of high valent metal ions to low valent metal ions could precipitate the metal ions efficiently, and thereby reduce the potential pollution of metal ions in natural environments.

The doping of metal or metal oxides could narrow the band gap, enhance the generation of e^--h^+ pairs and other free active species such as $\cdot O_2^-$ and ·OH radicals, promote the separation of e^--h^+ pairs and transfer the free active radicals, which increase the photocatalytic

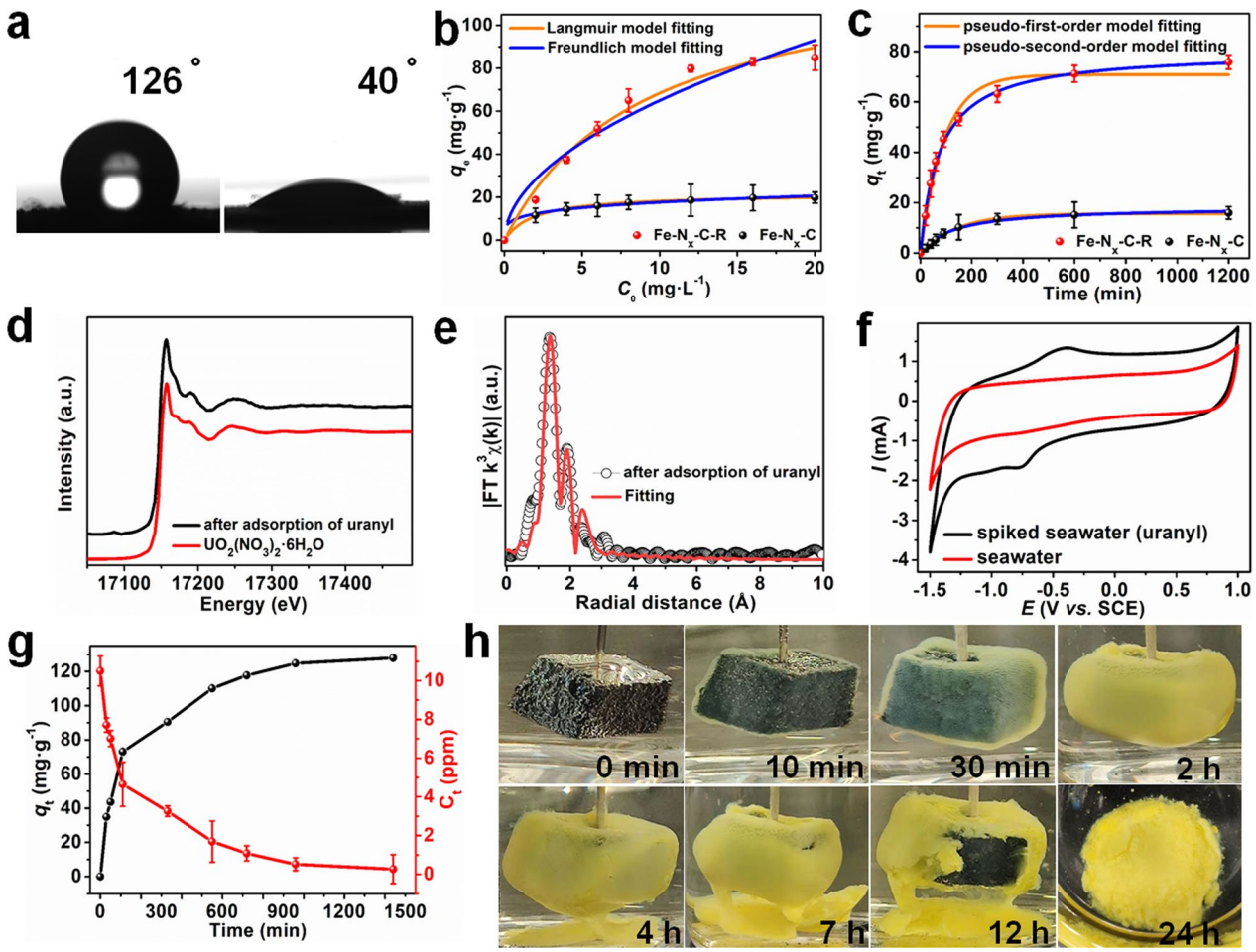

Fig. 3 **a** Contact angles for deionized water on pressed pellets of Fe—N_x—C (left) and Fe—N_x—C—R (right). **b** Equilibrium adsorption isotherms for uranyl ion adsorption on different materials at a fixed material—to—solution ratio of 0.1 mg·mL^{-1} in uranyl—spiked seawater (from 0 to 20 ppm). **c** Uranyl ion adsorption kinetics on different materials at an initial UO_2^{2+} concentration of 10 ppm in uranyl—spiked seawater. **d** U L_{III}—edge XANES spectra for Fe—N_x—C—R after adsorption of uranyl, and $UO_2(NO_3)_2·6H_2O$. **e** U L_{III}—edge EXAFS R—space and corresponding fitting curves for Fe—N_x—C—R after adsorption of uranyl. **f** Cyclic voltammograms for uranyl—spiked seawater and natural seawater. **g** Uranium extraction from spiked seawater with initial uranium concentrations of ~ 10 ppm, using Fe—N_x—C—R as an adsorbent—electrocatalyst. **h** Photographs of the Fe—N_x—C—R electrode in spiked seawater (initial uranium concentration of ~ 1000 ppm) during electrocatalytic extraction (Yang et al. 2021a)

performance of the biochar-based catalysts (Fang et al. 2021). The high stability, reusability and environmentally friendly properties suggest that biochar and biochar-based composites are promising materials in the removal or in-situ solidification/immobilization of heavy metal ions from aqueous solutions or in solid phases.

3 Organic pollutants

Photocatalytic degradation of OPs is one of the most efficient methods to decontaminate the organic pollution, especially at extra low concentrations (Yao et al. 2021; Zou et al. 2022). Ndoun et al. (2021) prepared biochar from guayule bagasse and cotton gin waste, and applied it for the adsorption of pharmaceuticals from solutions. The results showed that hydrophobic partitioning, H-bonding and π–π electron donor–acceptor interaction were the three mechanisms for pharmaceuticals' adsorption. With the increase of pyrolysis temperature, the surface hydrophobicity, zero-point charge value and surface area increased, which facilitated the binding the organic molecules on biochar. Ouyang et al. (2019) studied the defect structures of biochar on the photocatalytic performance. The biochar was synthesized under oxygen limited pyrolysis temperatures, the pyrolysis temperature had significant influence on biochar potency to active peroxymonosulfate. The degradation of 1,4-dioxane

increased from 4 to 84% when the pyrolysis temperature of biochar increased from 300 to 800 °C. The ESR, XPS, FTIR and Raman analyses indicated that the biochar defect contributed to the generation of OH and $SO_4$and O-containing groups were eliminated at high pyrolysis temperature, generating more defects and enhancing the biochar catalytic performance. The biochar activating peroxymonosulfate is a promising technique for the efficient remediation of organic contaminated water. Fang et al. (2017) studied the photochemical reduction of diethyl phthalate in biochar suspension under UV light irradiation. The singlet oxygen ($^1O_2$) and hydroxyl radicals (·OH) were the dominant reactive oxygen species for the reduction of diethyl phthalate. The electron paramagnetic resonance and free radical quenching analysis showed that biochar carbon matrix (BCM) generated about 64–74% ·OH and 10–45% $^1O_2$, whereas DOM derived from biochar accounted for 47–86% $^1O_2$ and 3.7–12% ·OH. The DOM derived from biochar contributed to the formation of $^1O_2$ and ·OH, the BCM formed excited triplet states and generated $^1O_2$ and superoxide radicals ($\cdot O_2^-$) and further yielded H_2O_2. The photo-Fenton reaction and BCM-bound persistent free radicals' activation generated ·OH radicals. The abovementioned possible pathways contributing to the degradation of diethyl phthalate are shown in Fig. 4a.

3.1 Ti-based biochar

Hu (2022) prepared N-doped TiO_2/biochar composites and compared the photocatalytic degradation of cephalosporin antibiotics with TiO_2 and TiO_2/biochar composites, and the results showed much higher photocatalytic degradation ability than the other two materials. The photoelectrochemical catalytic degradation is much superior to photocatalysis and electrocatalysis degradation of pollutants. Yang et al. (2021b) prepared phosphoric acid-modified biochar@TiO_2 (PMBC@TiO_2) composites and applied them for the removal of sulfadiazine from wastewater. The adsorption of sulfadiazine was spontaneous and endothermic, which was dominated by microporous binding, H-bonding, π–π interaction and electrostatic attraction. The surface adsorbed sulfadiazine could be quickly photocatalytic degraded under visible and UV light irradiation. The conjugated structure and O-containing groups promoted the efficient separation of e^--h^+ pairs and the generation of free $\cdot O_2^-$ and ·OH free radicals, which improved the photocatalytic capacity of the composites. Lu et al. (2019) prepared TiO_2/biochar for the photodegradation of methyl orange (MO), and found that the TiO_2/biochar catalyst exhibited much higher catalytic activity than TiO_2 with high stability and reusability. The decolorization and mineralization efficiencies of the TiO_2/biochar increased 21% and 51%, respectively, as compared to TiO_2. The photocatalytic degradation of MO is shown in Fig. 4b. Fazal et al. (2020) synthesized biochar-TiO_2 composite and applied it for photocatalytic degradation of simulated textile wastewater. The composite showed high separation of e^--h^+ pairs, slow recombination of e^--h^+ pairs, high visible light absorption and narrow band gap, which resulted in 99% degradation efficiency, much higher than those of biochar (85%) and TiO_2 (43%). The generated free $\cdot O_2^-$ and/or ·OH free radicals reacted with MB molecules and broke MB molecules to less toxic molecules or other products such as CO_2 and H_2O. The biochar acted as MB molecule adsorbent and provided efficient electron pathway through Ti–O–C bonds for photoexcited electrons to react with O_2 to form $\cdot O_2^-$. Cai et al. (2018) synthesized TiO_2/biochar composite and applied it for the photodegradation of safranine T (ST) under visible light irradiation. The binding of ST to the composite was mainly attributed to H-bond, π-π interaction and electrostatic attraction, which is similar to most published papers. The photodegradation of ST was the free active species of $\cdot O_2^-$ and ·OH, also similar to the results of Fazal et al. (2020). The photocatalytic degradation of MB by TiO_2/biochar was mainly dominated by hydroxyl radicals (·OH) (Silvestri et al. 2020), a little difference with the abovementioned TiO_2/biochar catalyst for MB and ST. Nevertheless, the photocatalytic degradation of OPs is mainly attributed to the active species of $\cdot O_2^-$ and ·OH, and the free electrons and holes. The TiO_2/biochar composites showed much higher sulfamethoxazole removal and mineralization than TiO_2 and biochar. The enhancement of sulfamethoxazole removal was due to hydrophobic interaction between sulfamethoxazole and biochar, whereas the enhanced photocatalytic degradation was attributed to the low recombination of e^--h^+ pairs, efficient attachment of e^--h^+ pairs to TiO_2 and high adsorption of sulfamethoxazole to biochar (Kim and Kan 2016). Zhang et al. (2017) synthesized TiO_2/biochar catalyst and applied it for the removal of sulfamethazine from wastewater. The catalyst showed high photocatalytic capacity after five cycles, and the biochar could promote the separation of e^--h^+ pairs. The hydroxylation, cleavage of N-S bond and opening of isoxazole rings contributed to the photocatalytic degradation of sulfamethazine.

3.2 Fe-based biochar

Zhai et al. (2020) prepared biochar@$CoFe_2O_4$/Ag_3PO_4 composites and applied them for the photocatalytic degradation of bisphenol A (BPA) under visible light irradiation and showed high catalytic activity and stability. The intermediates and final products were measured by GC–MS and the photocatalytic degradation mechanism was proposed in Fig. 4c. Zhang et al. (2021b) prepared

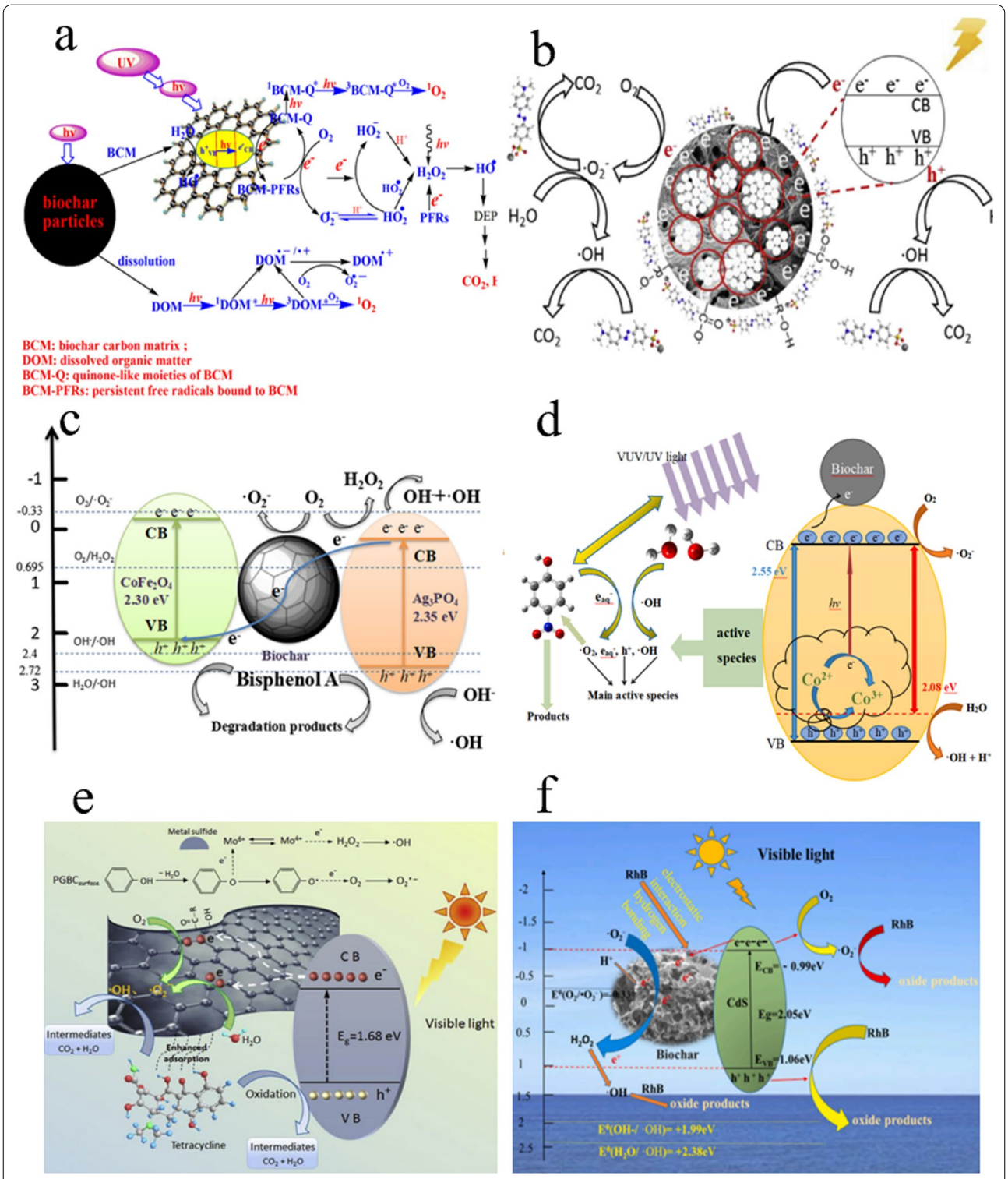

Fig. 4 Possible pathways for the degradation of diethyl phthalate photodegradation by biochar (**a**) (Fang et al. 2017); Photodegradation mechanism of MO by TiO_2/biochar (**b**) (Lu et al. 2019); Photocatalytic degradation mechanism of BPA by biochar@$CoFe_2O_4$/Ag_3PO_4 composites (**c**) (Zhai et al. 2020); Photocatalytic degradation of p-nitrophenol by Co(II)-doped BiOCl@biochar (**d**) (Cao et al. 2021); Photodegradation mechanism of TC by MoS_2/biochar under sunlight (**e**) (Ye et al. 2019); Photodegradation of RhB by CdS/biochar under visible light irradiation (**f**) (Kang et al. 2022)

FeOOH/Fe_3O_4/biochar with high magnetic and photocatalytic activities, and applied it for the removal of MO from aqueous solutions. The composites showed 2.03 times of MO photodegradation activity higher than biochar although the surface area of the composite was much lower than that of biochar. The ESR and free radical quenching analysis showed that ·OH radicals were the primary species for the photocatalytic degradation of MO. More importantly, the catalysts showed high stability and reusability with at least 98% photocatalytic activity after 5 cycles, and can be easily separated from solution by magnetic separation technique. Huang et al. (2022) prepared nZVI/biochar and used it to activate PMS for sulfamethazine degradation. The catalyst had rich pores, defective structures and high graphitization, which resulted in high catalysis performance. The catalyst could degrade ~ 100% sulfamethazine in 20 min with high catalytic capacity and reusability. The EPR, quenching and XPS analyses showed that nonradical and radical pathways acted in sulfamethazine degradation, and the nZVI, pyridinic N, –COH and –COOH groups were the main active sites for the binding of sulfamethazine.

3.3 Bi-based biochar

Kumari et al. (2021) synthesized bismuth-modified biochar for photodegradation of MB and showed 90% degradation of MB, which was attributed to high adsorption of MB and efficient separation of e^--h^+ pairs. However, the authors did not discuss the results in detail and the relative contribution of reactive free species was even not identified. Co(II)-doped BiOCl@biochar composite showed 99% photocatalytic degradation of p-nitrophenol in 90 min with high stability and recycle reusability, and 5% Co(II) doping in 30% biochar loading had the highest photocatalytic ability. The addition of BiOCl in biochar narrowed the band gap, enhanced light absorption, increased the separation of photogenerated e^--h^+ pairs and thereby increased the photocatalytic performance. The photocatalytic degradation mechanism is shown in Fig. 4d (Cao et al. 2021).

3.4 Zn/Co-based biochar

Goncalves et al. (2020) synthesized ZnO/biochar under different temperatures and applied them for the degradation of MO and sulfamethoxazole antibiotic (SMX), and compared the degradation capacity of the samples. The results showed that the photocatalytic activity is dependent on the pyrolysis temperature, which affected the band gap energy and visible light absorption efficiency. Yu et al. (2021b) synthesized ZnO/biochar by ball milling method. The biochar was broken in ball milling process, and the meso- and macropores of the composites were increased, which enhanced the adsorption of MB on the composites. 95% MB was removed under visible light conditions through adsorption and photocatalytic degradation. The electrons were generated and then reacted with O_2 to form $\cdot O_2^-$ free radicals, which facilitated the degradation of MB. Welter et al. (2022) prepared $ZnFe_2O_4$/biochar composites and applied them for the degradation of RhB using heterogeneous photo-Fenton processes. Siara et al. (2022) applied $ZnAl_2O_4$-biochar for the degradation of ibuprofen, and found that 100% ibuprofen (20 mg/L) was eliminated in 120 min, which was attributed to the high surface area, pore volume and mesoporous size of $ZnAl_2O_4$-biochar. The free $\cdot O_2^-$ and ·OH radicals contributed to the photocatalytic degradation of ibuprofen into by-products with lower molecular weight. Gholami et al. (2020) incorporated Zn-Co-LDH with biochar and used it for gemifloxacin photodegradation. 93% gemifloxacin was degraded in 130 min at the initial concentration of 15–35 mg/L. The free radical scavenging experiments showed the contribution of the radical species to gemifloxacin degradation in the sequence of $\cdot OH > h^+ > O_2^-$. Yang et al. (2021c) applied N-doped biochar for the photodegradation of sulfamethazine and found that $^1O_2$ was the main active species for sulfamethazine degradation from the ESR and quenching measurements. Further DFT calculation indicated that the pyridinic N-doping decreased the intersystem crossing energy and thereby benefited $^1O_2$ generation by energy transfer and electron transfer.

3.5 Mo/Cd-based biochar

Ye et al. (2019) prepared porous graphite biochar assembled with MoS_2 nanosheets, which have high graphitization degree and porosity, suitable band gap for visible light absorption, efficient separation of e^--h^+ pairs and charge transfer acceleration. The batch experiments showed that adsorption of tetracycline hydrochloride (TC) was dominated by H-bonding, π–π interaction, electrostatic attraction and pore filling, whereas the photocatalytic degradation was mainly dominated by the hydroxy radicals (·OH) and holes (h^+) (Fig. 4e). The composites showed much higher adsorption capacity and photocatalytic ability than biochar and MoS_2, and the high stability and reusability indicated that the composites could be used as potential catalysts in the efficient degradation of OPs.

Kang et al. (2022) prepared sulphur-modified biochar/CdS composites and applied them for the adsorption-photocatalytic degradation of RhB under visible light irradiation. The composites showed high adsorption of RhB because of the large surface area and abundant active sites, and promoted the separation and utilization of photogenerated e^--h^+ pairs. The electrostatic interaction and H-bonding were the main mechanisms for the

uptake of RhB, whereas the superoxide radicals ($\cdot O_2^-$) contributed mainly to the photodegradation of RhB from the quenching tests and EPR analysis. The mechanism for the generation of active radicals for RhB degradation was illustrated in Fig. 4f.

3.6 Ag-based biochar

Wang et al. (2019b) synthesized Ag nanoparticle-doped biochar/$Bi_4Ti_3O_{12}$ to improve the photocatalytic performance. The doped Ag could promote the separation of electrons and holes, and the biochar could provide chemical groups to improve electron transfer. The surface doping of metal nanoparticles is an efficient strategy to improve the photocatalytic capacity. Wei et al. (2021) synthesized Ag_3PO_4/biochar catalyst. The Ag_3PO_4 nanoparticles were well dispersed in the porous structure of biochar and Ag^0 nano-species were generated in the catalyst. The Ag^0 nano-species could act as a bridge to transfer the photogenerated electrons quickly from Ag_3PO_4 to biochar, and then reacted with the adsorbed O_2 to produce ·OH active radicals. The Ag_3PO_4/biochar showed high photocatalytic capacity in the degradation of MB, and 96% MB was efficiently removed in 60 min under visible light conditions. From the abovementioned results, one can see that the doping of metal nanoparticles could enhance the photocatalytic performance of biochar-based composites because of the high generation and separation of free active radicals, electrons and holes, and high adsorption ability of pollutant molecules on biochar.

3.7 C_3N_4-based biochar

Xiao et al. (2021) prepared C_3N_4/biochar and applied for for the removal of enrofloxacin through adsorption and photocatalysis strategy. The composite showed much higher adsorption and photodegradation capacities to enrofloxacin with higher stability and reusability than pure C_3N_4 and biochar. The $\cdot O_2^-$ and h^+ were the main species for the photocatalytic degradation of enrofloxacin. The g-C_3N_4/biochar showed much higher photodegradation of formaldehyde than g-C_3N_4 under visible light conditions, which was attributed to increased specific surface area and separation of e^--h^+ pairs by chrysanthemum g-C_3N_4 and visible light absorption by biochar skeleton (Li et al. 2019b). Karpuraranjith et al. (2021) synthesized magnetic biochar-based C_3N_4 catalyst, and applied for the photodegradation of RhB dye under visible light conditions. The composite showed much higher photocatalytic performance than biochar and C_3N_4 with outstanding recyclability, stability and eco-friendliness. The efficient separation of photogenerated e^--h^+ pairs and effective suppress of e^--h^+ pairs recombination enhanced the photocatalytic capacity. The reactive $\cdot O_2^-$ and ·OH free radicals contributed to the RhB degradation. The biochar/C_3N_4 composites also showed much higher adsorption capacity to cationic MB dye and high photocatalytic degradation of MB, which was attributed to the oxidative species of superoxide anion radicals and photogenerated e^--h^+ pairs (Pi et al. 2015). Kumar et al. (2017) prepared g-C_3N_4/$FeVO_4$/Fe@NH_2-Biochar and applied it for the removal of methyl paraben and 2-cholrophenol through adsorption, photodegradation and photo-ozonation strategy. The catalyst showed high surface area, porous nanosheet structure, high stability, broad solar light absorption and good separation of e^--h^+ pairs. The $FeVO_4$ and Fe were favorable for higher light absorption and thereby increased the photocatalytic activity. The elimination of the two organic contaminants was carried out under four conditions, i.e., photodegradation, adsorption followed by photodegradation; simultaneous adsorption and photodegradation (SAP); and SAP plus O_3 photo-ozonation. The results showed that adsorption and photodegradation was a good method for high elimination of organic contaminants, whereas the adsorption, photodegradation plus photo-ozonation showed a little higher efficiency than the other three methods. The photo-ozonation could accelerate the degradation rate and shorten the reaction time.

3.8 Mixed metal-based biochar

Azalok et al. (2021) synthesized MnFe-LDO-biochar and applied it to remove tetracycline from solutions. Under dark condition, 40% tetracycline (20 mg/L) was removed in 30 min, whereas 98% tetracycline was eliminated in 240 min under UV light irradiation. In the presence of $K_2S_2O_8$ and H_2O_2, 98% tetracycline could be removed in 60 min. The photodegradation of tetracycline was mainly attributed to the ·OH and $\cdot SO_4^-$ active species, whereas the mineralization was dominated by $\cdot O_2^-$ and h^+. The biochar/$ZnFe_2O_4$/BiOBr showed much higher photocatalytic degradation of ciprofloxacin than $ZnFe_2O_4$ and BiOBr under visible light irradiation. The $ZnFe_2O_4$ and BiOBr could promote the separation of photogenerated e^--h^+ pairs as $ZnFe_2O_4$ and BiOBr could serve as heterojunctions. The high adsorption ability of biochar, efficient separation of e^--h^+ pairs and prolonged recombination time of e^--h^+ pairs resulted in the high photocatalytic degradation ability of biochar/$ZnFe_2O_4$/BiOBr with high stability and reusability (Chen et al. 2019b). Peng et al. (2021) synthesized $ZnFe_2O_4$/B,N-codoped biochar and applied it for enhancing adsorption-photodegradation of tetracycline hydrochloride (TCH) from solutions. The results showed that 98% TCH (150 mg/L) was removed from solutions in 120 min with the adsorption capacity of 244 mg/g. The B and N doping mass affected the adsorption and photocatalytic degradation efficiency of the composites. The relative contribution of the ·OH, e^-,

h^+ and $\cdot O_2^-$ active species to the degradation of TCH was evaluated by free radical quenching tests. The e^- and $\cdot O_2^-$ were vital for the photodegradation of TCH, which was also evidenced in the ESR spectra where the intensity of $\cdot O_2^-$ was much stronger than that of ·OH. The photocatalytic degradation efficiency decreased from 98 to 89% after seven cycles, suggesting the relative stability and recyclability of the composites in the efficient elimination of TCH from aqueous solutions. Talukdar et al. (2020) synthesized Ag_3PO_4/Fe_3O_4-biochar with high stability and magnetic property. The photocatalytic degradation of bisphenol A (BPA) by the catalyst in peroxydisulfate system was carried out under visible light condition, and 96% BPA was degraded after 60 min, which was mainly attributed to $\cdot O_2^-$, $\cdot SO_4^-$, and ·OH active species.

Khataee et al. (2019) prepared Cu_2O-CuO@biochar and applied it for the photodegradation of reactive orange 29 (RO29). 94% RO29 (20 mg/L) was degraded at pH 8.9 in 90 min. The by-products were measured by GC–MS and the by-products were finally mineralized to H_2O, CO_2 and inorganic ions. Navarathna et al. (2020) synthesized magnetic MOF/biochar catalyst and applied it for the photodegradation of RhB in the absence and presence of Cr(VI). The adsorption of RhB to the catalyst was mainly dominated by electrostatic attraction and π–π interaction. The presence of Cr(VI) increased the photocatalytic degradation of RhB, and Cr(VI) was also photo-reduced to Cr(III). However, the relative contribution of the free active radicals to the photodegradation of RhB was not discussed in detail, especially from ESR and quenching analysis. The photocatalytic degradation of different OPs using different biochar-based catalysts was summarized in Table 2. From Table 2, one can see that the main active species for the degradation of different OPs are quite different, even for similar biochar-based catalyst for the photodegradation of same pollutant molecules. Nevertheless, the photocatalytic degradation of organic molecules was mainly dominated by the photogenerated electron–hole pairs, free $\cdot O_2^-$, and ·OH active radicals.

Till now, the photocatalytic degradation of different OPs has been extensively studied using different kinds of biochar-based catalysts. The sources for the synthesis of biochar, the pyrolysis temperature and the conditions for the preparation of biochar affect the structures, surface functional groups, band gap, surface areas and inner-pore properties, which thereby influence the photocatalysis performance of biochar and biochar-based materials. The doping of metal or metal oxides is the main strategy to improve the photocatalytic performance of biochar-based catalysts. The doping of metal or metal oxides could narrow band gap, enhance the generation and separation of photogenerated electron–hole pairs, increase the absorption of visible light etc. It is necessary to note that the amount of metal or metal oxides in the composites, the types of metals, single or multi-doping of metals also influence the photocatalytic properties of biochar-based catalysts. The catalysts could simultaneously remove OPs through adsorption-photodegradation processes.

For the photodegradation of different OPs, the relative contributions of different free active species are a little different, which is mainly attributed to the generation of the free active radicals by different composites. One can speculate the degradation mechanism of OPs from ESR, quenching tests and other advanced spectroscopy analysis. However, the analysis of intermediate products and the exactly contribution of each active radicals to the photodegradation is still a challenge, which is helpful to construct the catalysts.

4 Mechanism discussion

4.1 Advanced spectroscopy analysis

The interaction mechanism of pollutants with biochar or biochar-based catalysts is dependent on the properties of materials (i.e., structures, surface functional groups, band gap, light absorption ability, (photo)catalytic performance, stability etc.) and the properties of pollutants (i.e., oxidation–reduction reactions, species, bond strength, coordination properties, structures of pollutants etc.). The interaction of OPs with biochar is generally dominated by electrostatic attraction, hydrophobic effect, H-bonding and π–π interaction etc., whereas the interaction of inorganic pollutants is generally attributed to ion exchange, surface complexation, (co)precipitation etc. The surface adsorbed organic molecules could be photocatalytic degraded by the photogenerated e^--h^+ pairs, free $\cdot O_2^-$ or ·OH active free radicals, and the metal ions could be reduced from high valence to low valence, which could be in-situ solidified on solid particles. Different kinds of spectroscopy techniques such as XPS, FTIR, Raman and XAFS have been applied to understand the interaction of pollutants. In the FTIR or XPS spectra, from the appearance of new peaks, the disappearance of peaks, change of peak intensities, the red/blue shift of peaks, one can achieve some useful information about the interaction of pollutants with the functional sites/groups, although such information is semi-qualitatively. From the XAFS analysis, one can get some information about the structures of metal ions such as the coordination number and bond distance with the atoms around the metal ions at molecular level, the oxidation–reduction state of the metal ions etc. The in-situ analysis could provide the dynamic interaction process information, such as the change of species with the change of interaction time. Liu et al. (2022b) applied in-situ electrochemical Raman system (Fig. 5a) to measure the U(VI) species and the formation of U(VI) precipitates as a function of reaction time

Table 2 Summary of biochar-based catalysts in the photocatalytic degradation of organic pollutants

Catalysts	Pollutants	Mechanisms and main active radicals	References
Biochar	Diethyl phthalate	Singlet oxygen ($^1O_2$) and hydroxyl radicals (·OH) were main active species for photoreduction	Fang et al. (2017)
Biochar	Pharmaceutical	Adsorption was dominated by hydrophobic partitioning, H-bonding and π–π electron donor–acceptor interaction	Ndoun et al. (2021)
TiO_2-biochar	Cephalosporin antibiotics	Photoelectrochemical catalytic degradation	Hu (2022)
TiO_2-biochar	Sulfadiazine	Adsorption was dominated by microporous binding, H-bonding, π–π interaction and electrostatic attraction. Photodegradation was dominated by e^--h^+ pairs, free $\cdot O_2^-$ and ·OH radicals	Yang et al. (2021b)
TiO_2-biochar	Methyl orange	e^--h^+ pairs, free $\cdot O_2^-$ and ·OH radicals contributed to the degradation	Lu et al. (2019)
TiO_2-biochar	Methyl blue	Ti–O-C bonds provided electron pathways for electrons to react with O_2 to form $\cdot O_2^-$. Free $\cdot O_2^-$ and ·OH radicals contributed to MB photocatalytic degradation	Fazal et al. (2020)
TiO_2-biochar	Safranine T	Adsorption was dominated by H-bond, π-π interaction and electrostatic attraction. Photodegradation was dominated by free $\cdot O_2^-$ and ·OH species	Cai et al. (2018)
C_3N_4-biochar	Enrofloxacin	The $\cdot O_2^-$ and h^+ were the main species for the photocatalytic degradation of enrofloxacin	Xiao et al. (2021)
Magnetic C_3N_4-biochar	RhB	Photodegradation was dominated by e^--h^+ pairs, free $\cdot O_2^-$ and ·OH radicals	Karpuraranjith et al. (2021)
C_3N_4-biochar	Methyl blue	Photodegradation was dominated by e^--h^+ pairs, free $\cdot O_2^-$	Pi et al. (2015)
$CoFe_2O_4/Ag_3PO_4$-biochar	Bisphenol A	Photodegradation was dominated by e^--h^+ pairs, free $\cdot O_2^-$ and ·OH radicals	Zhai et al. (2020)
ZnO-biochar	Methyl orange	Photodegradation was dominated by e^--h^+ pairs, free $\cdot O_2^-$ radicals	Yu et al. (2021b)
$ZnAl_2O_4$-biochar	Ibuprofen	Free $\cdot O_2^-$ and ·OH radicals contributed to the photocatalytic degradation	Siara et al. (2022)
MoS_2-biochar	Tetracycline hydrochloride	Adsorption was dominated by H-bonding, π-π interaction, electrostatic attraction and pore filling. Photocatalytic degradation was mainly dominated by ·OH and holes (h^+)	Ye et al. (2019)
CdS-biochar	RhB	Adsorption was dominated by electrostatic interaction and H-bonding. Photodegradation was mainly dominated by superoxide radicals ($\cdot O_2^-$)	Kang et al. (2022)
Zn-Co-LDH-biochar	Gemifloxacin	The degradation was mainly dominated by ·OH, h^+ and $\cdot O_2^-$ free radicals, and in the sequence of ·OH > h^+ > $\cdot O_2^-$	Gholami et al. (2020)
$FeOOH/Fe_3O_4$-biochar	Methyl orange	·OH radicals were the primary species for the photocatalytic degradation of MO	Zhang et al. (2021b)
MnFe-LDO-biochar	Tetracycline	Photodegradation was mainly attributed to ·OH and $\cdot SO_4^-$ active species. Mineralization was dominated by $\cdot O_2^-$ and h^+	Azalok et al. (2021)
$ZnFe_2O_4$/B,N-codoped biochar	Tetracycline hydrochloride	Photodegradation was mainly attributed to ·OH, e^- and $\cdot O_2^-$ species	Peng et al. (2021)
Ag_3PO_4/Fe_3O_4-biochar	bisphenol A	Photodegradation was mainly attributed to $\cdot O_2^-$, $\cdot SO_4^-$, and ·OH active species	Talukdar et al. (2020)

*It is necessary to note that although the names of some catalysts are the same, they are not the same materials

in the adsorption-electrocatalytic reduction process. The Raman peak at 489 cm^{-1} suggested the presence of adsorbed U(VI) on the electrode (Liu et al. 2017). With the increase of reaction time, the peak at 489 cm^{-1} disappeared whereas a signal at 810 cm^{-1} appeared, suggesting the reduction of U(VI) to U(V) (Pointurier and Marie 2013; Stefaniak et al. 2008). New Raman peak at 374 cm^{-1} appeared in the Raman spectrum at 240 s, indicating the formation of unstable U(V) to stable U(VI) on electrode, forming $Na_2O(UO_3{\cdot}H_2O)_x$ precipitate (Fig. 5b). The in-situ Raman analysis clearly showed the change of U(VI) species as a function of contact time. The XAFS analysis showed that a U atom was coordinated with 2 axial O atoms and 4 square planar O atoms with the U–O bond distances of ~ 1.8 Å and ~ 2.2 Å, respectively, which is in good agreement with the results of in-situ Raman analysis. The good agreement of different spectroscopy

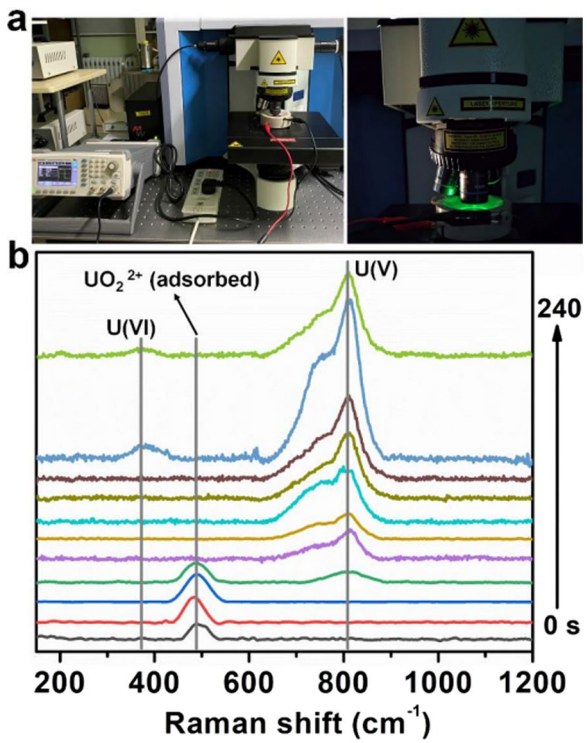

Fig. 5 **a** Photographs showing the in situ electrochemical—Raman microscope system. **b** In situ Raman spectra collected from the In—Nx—C—R/carbon felt working electrode in uranium—spiked seawater during the adsorption—electrocatalysis process (Liu et al. 2022b)

characterization could confirm the interaction mechanism more exactly rather than one spectroscopy analysis.

For organic molecular photocatalytic degradation, the relative contributions of active free radicals to the degradation processes are usually determined from the electron paramagnetic resonance (EPR) analysis. The light absorption can be measured by UV–vis diffuse reflection spectroscopy (UV–vis DRS) directly, which is helpful to evaluate the electronic structures of catalysts. Generally, there are four main steps in organic molecule degradation, i.e., (1) light absorption to generate e^--h^+ pairs; (2) efficient separation of e^--h^+ pairs; (3) to transfer the holes and electrons to catalyst surface and to avoid the e^--h^+ recombination; and (4) the degradation of organic molecules by the generated active radicals (Qiu et al. 2021). The free active species such as $\cdot O_2^-$, $^1O_2$, ·OH, h^+ etc. can be evaluated through the addition of radical scavengers. Quenching tests are generally carried out to evaluate the relative contribution of active free radicals. The degradation of different OPs by biochar-based catalysts through the addition of different radical scavengers is shown in Fig. 6a (Talukdar et al. 2020). One can see that the photocatalytic degradation of BPA was obviously inhabited after the addition of TBA, MeOH or BQ. The addition of BQ could scavenge $\cdot O_2^-$ radicals, whereas the addition of TBA or MeOH could scavenge ·OH or $\cdot SO_4^-$/·OH, respectively. The effect of the radical trapping scavengers was in the order of TBA < MeOH < BQ, suggesting the contribution of $\cdot O_2^-$ radicals was much stronger than that of ·OH or $\cdot SO_4^-$ radicals. However, the total contribution of the free active species on the photocatalytic degradation of BPA is > 100%, suggesting the contribution of the free active radicals is dependent on each other and the quantitative contribution of each free radicals is not calculated accurately. The EPR spectroscopy is generally used to measure the generation of reactive free radicals. No signal was found for dark conditions, and the signals of $\cdot O_2^-$ radicals were found for BC300 (biochar heated at 300 °C) and BM300 (BC300 was treated by ball milling) samples (Fig. 6b) (Xiao et al. 2020). The signal intensity of BC300 was weaker than that of BM300, suggesting more generation of $\cdot O_2^-$ radicals by BM300, which is in good agreement with the results that the photocatalytic performance of BM300 was stronger than that of BC300.

The influences of photogenerated electron migration on the degradation should also be considered. Once excited by light, photogenerated electrons (e^-) and holes (h^+) are generated in the desired photocatalysts, which directly participate in surface redox reactions through different routes. The separation and transfer of charge carriers, especially for photogenerated e^-, play a vital role during photocatalysis. The rational regulation of photogenerated e^- migration not only benefits for the separation of charge carriers, but also prolongs their lifetimes for photoreactions (Zhang et al. 2019a). For example, after the doping of strongly electronegative O atoms (Fig. 6c), more electrons and holes were separately gathered onto the aromatic ring planes of g-C_3N_4 by forming the e^- and h^+-related delocalized systems. As a result, more reactive species were yielded forthe removal of refractory organic pollutants. In addition, the surface functionalization can induce the directional transfer of photogenerated e^- from the bulk to reaction centers, which shortens their transmission distances and reduces mass transfer losses. Thus, the utilization of photogenerated e^- and optical quantum efficiency will be significantly improved. As previously reported, hydroxyl groups (–OH) and cyano groups (–C≡N) as electron-withdrawing groups were engineered into mesoporous g-C_3N_4 (Fig. 6d), which served as reaction sites to capture and directionally transport electrons from photocatalysts to persulfates (electron acceptors) (Zhang et al. 2019b). Benefiting from the unidirectional transfer, plenty of strong oxidized $SO_4^{\cdot-}$ radicals were produced from efficient photoreduction of $S_2O_8^{2-}$ anions and then attacked organic pollutant molecules till

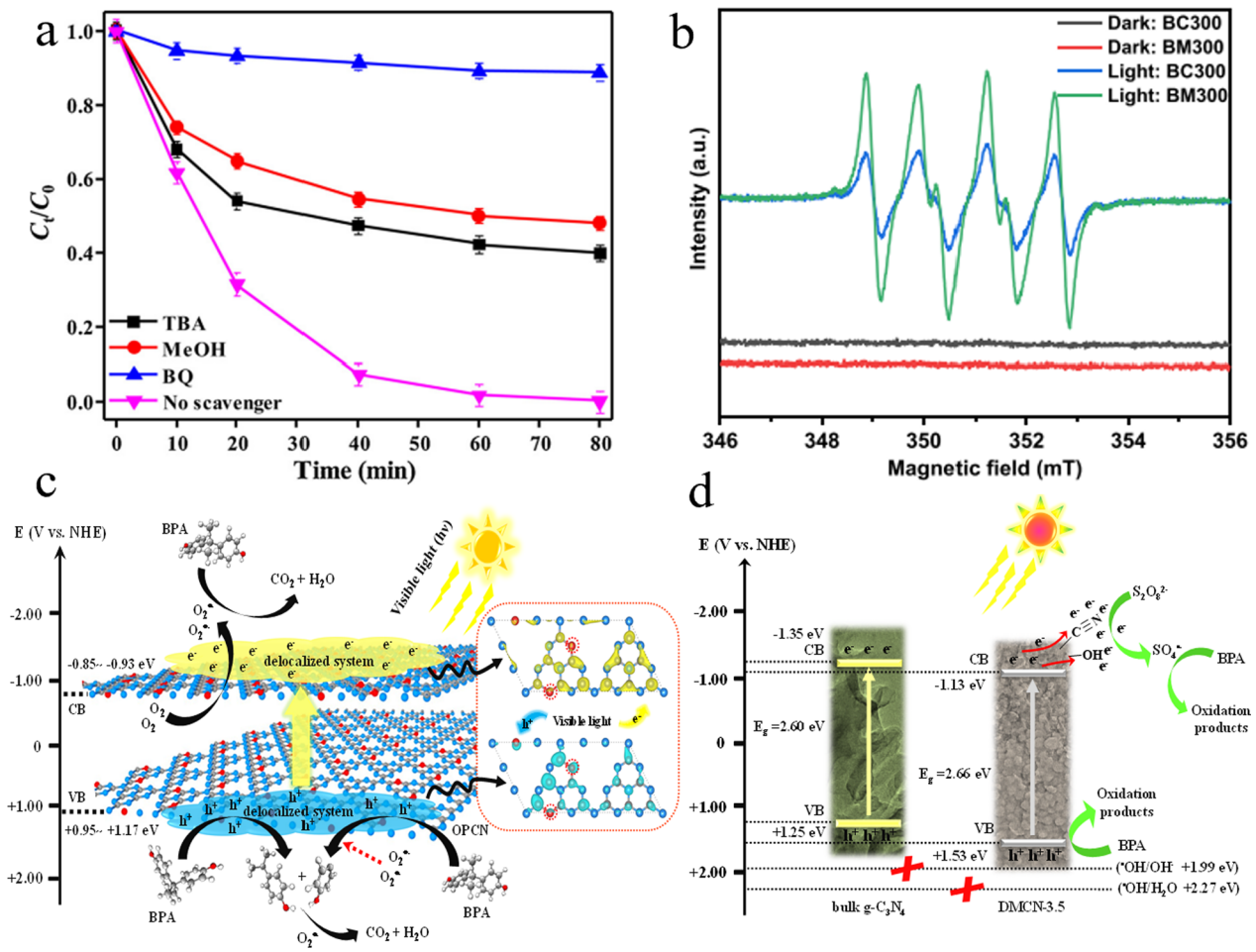

Fig. 6 **a** Effect of radical scavengers on photocatalytic degradation of BPA in the Vis/Ag–Fe@BAB/PDS system (Talukdar et al. 2020); **b** DMPO-·O_2^- concentration of BC300 and BM300 in methanol dispersion under dark and light conditions (Xiao et al. 2020); Schematic diagrams for photogenerated electron migration in **c** OPCN (Zhang et al. 2019a) and (**d**) DMCN (Zhang et al. 2019b) photocatalysts under visible light irradiation

their complete degradation. Synchronously, much more photogenerated holes remained on the valence band of photocatalysts for direct oxidation during reactions. In brief, the effective migration of photogenerated electrons will induce efficient separation of charge carriers and improve the utilization of solar energy.

For most literatures, the analysis of products was not carried out although the products could be measured from the liquid chromatography coupled to mass spectrometer (LC MS), and the intermediates can also be identified from LC MS analysis, which is helpful to propose the degradation mechanism (Siara et al. 2022). Nevertheless, the photocatalytic degradation mechanism of organic molecules is difficult to be confirmed. One can speculate the degradation routes from the analysis of intermediates and final products, from the measurements of free active radicals, and computational simulation to understand the possible degradation mechanism.

4.2 Computational calculation

As the structures of biochar are not well defined and the intermediates are difficult to be analyzed directly, computational simulation can be applied to simulate the possible degradation pathway. The reaction energies and intermediates can be simulated in DFT calculations, which is helpful to evaluate the photocatalytic degradation mechanism. The interaction between organic molecules and biochar-based catalysts can be simulated. The photocatalytic degradation of organic pollutants can be predicted and evaluated by computational calculation using different models (Wang et al. 2021). To our best knowledge, the DFT calculation about the photocatalytic degradation of organic molecules by biochar-based

catalysts is still scarce, which may be attributed to the complicated structures of biochar. The possible degradation of BPA, the structures of intermediates, transition states and interaction energies are simulated and the results are shown in Fig. 7a and b (Zhang et al. 2019a). In the DFT simulation, the possible intermediates with reaction energies and bond distances with different atoms such as C, N or O atoms are calculated, which is helpful to draw the possible photocatalytic degradation pathway. The impossible intermediates with very high reaction energies can also be calculated. The photoexcited state is also important to understand the degradation of organic molecules. The generated electrons and holes with charge distribution and density are calculated and shown in Fig. 7c. The free e^- transfer occurs to O atoms of Mo–O cluster, and the h^+ transfers reversely to C atoms, resulting in efficient separation of photogenerated e^--h^+ pairs and thereby improves the photocatalytic performance. The possible surface and interlayer adsorption of BPA and 4-CP are simulated (Fig. 7d). The structures and bond distances are also calculated, and the BPA is preferably adsorbed in the interlayer with –OH groups. The adsorption of 4-CP demonstrates that 4-CP tends to be adsorbed on the inserted Mo–O clusters by –OH groups (Zhang et al. 2022b). The DFT calculation proved that the O atoms in Mo–O clusters served as the adsorption sites, which is useful to understand the photocatalytic degradation of BPA, 4-CP or other kinds of organic molecules. Nevertheless, the DFT calculation could provide qualitative information about the interaction of organic molecules with catalysts. Although computational calculation of OPs with biochar or biochar-based catalysts is still scarce, the DFT calculation could be carried out to simplify the complicated structures of biochar. In near future, the DFT simulation of organic molecules interaction with biochar and biochar-based catalysts and the degradation pathway evaluation will attract extensively interest.

5 Conclusion and perspective

In this review article, we mainly summarized the recent works, especially in last five years, about the adsorption-photocatalytic degradation of organic contaminants and adsorption-(photo)catalytic reduction of heavy metal ions using biochar and biochar-based catalysts. Although biochar itself has high adsorption capacity, the low photocatalytic ability restricts the application of biochar as photocatalyst in real works. The heteroatom (i.e., S, N, P, B etc.) doping of biochar has fruitful effect to improve the photocatalytic degradation of biochar. The in-situ synthesis or post-modification strategies could achieve the heteroatom doping. The doping of metal or metal oxides on biochar is an effective strategy to narrow the band gap of the catalyst, to enhance the visible light absorption, to increase the generation and separation of photogenerated electron and hole pairs, and to produce more free active radicals, thereby increasing the photocatalytic properties of biochar-based catalysts. The environmentally friendly properties of biochar make it a suitable material in the photocatalytic degradation of organic contaminants or the (photo)reduction of metal ions and then immobilization of the metal ions to decrease the transport of metal ions in the natural environment.

In the photocatalytic degradation of organic contaminants or reduction of heavy metal ions, there are still many challenges in future, for example: (1) the relative contribution of active species is generally evaluated from ESR and quenching tests, which are helpful to understand the qualitative analysis of different free active radicals on the degradation/reduction of the environmental contaminants; (2) the quantitative analysis of the active species' contribution is still unclear. One can see that the sum of each free active radicals is much higher than 100%, suggesting the independent contribution of the active radicals. The relative qualitative contribution of free active radicals could be evaluated, but the quantitative contribution of each free radicals is not calculated accurately; (3) the whole degradation processes are still "black-box" as the intermediate products are difficult to be measured exactly. Computational calculation is a very useful technique to simulate the different degradation pathways, and to achieve the structures and transition state of reactants and intermediates. However, the structure of biochar is very complicated and it is really very difficult to construct the computational calculation mode. Till now, computational simulation of photocatalytic degradation/reduction of contaminants by biochar or biochar-based catalysts is still not available in large scale; (4) the toxicity of the catalyst should also be considered although biochar is environmentally friendly. The release of metals or metal oxides from the biochar-based catalyst is inevitably, which are generally

(See figure on next page.)

Fig. 7 DFT calculated structures of reactants, intermediates and transition state for the degradation of BPA attacked by OPCN catalysts with N atoms (**a**) or O atoms (**b**) as reactive sites (white, red, gray and blue balls represented H, O, C and N elements, respectively) (Zhang et al. 2019a); **c** Computed charge distributions on $[Mo_7O_{24}]^{6-}$-CN once being excited by visible light. Isodensity representation of the electron and hole were given in cyan and mauve, respectively; **d** The optimized structures for the adsorption of BPA and 4-CP on $[Mo_7O_{24}]^{6-}$-CN. Bond lengths were in Å. (The blue, gray, white, red, pale pink and green balls represented N, C, Mo, O, H, and Cl atoms, respectively) (Zhang et al. 2022b)

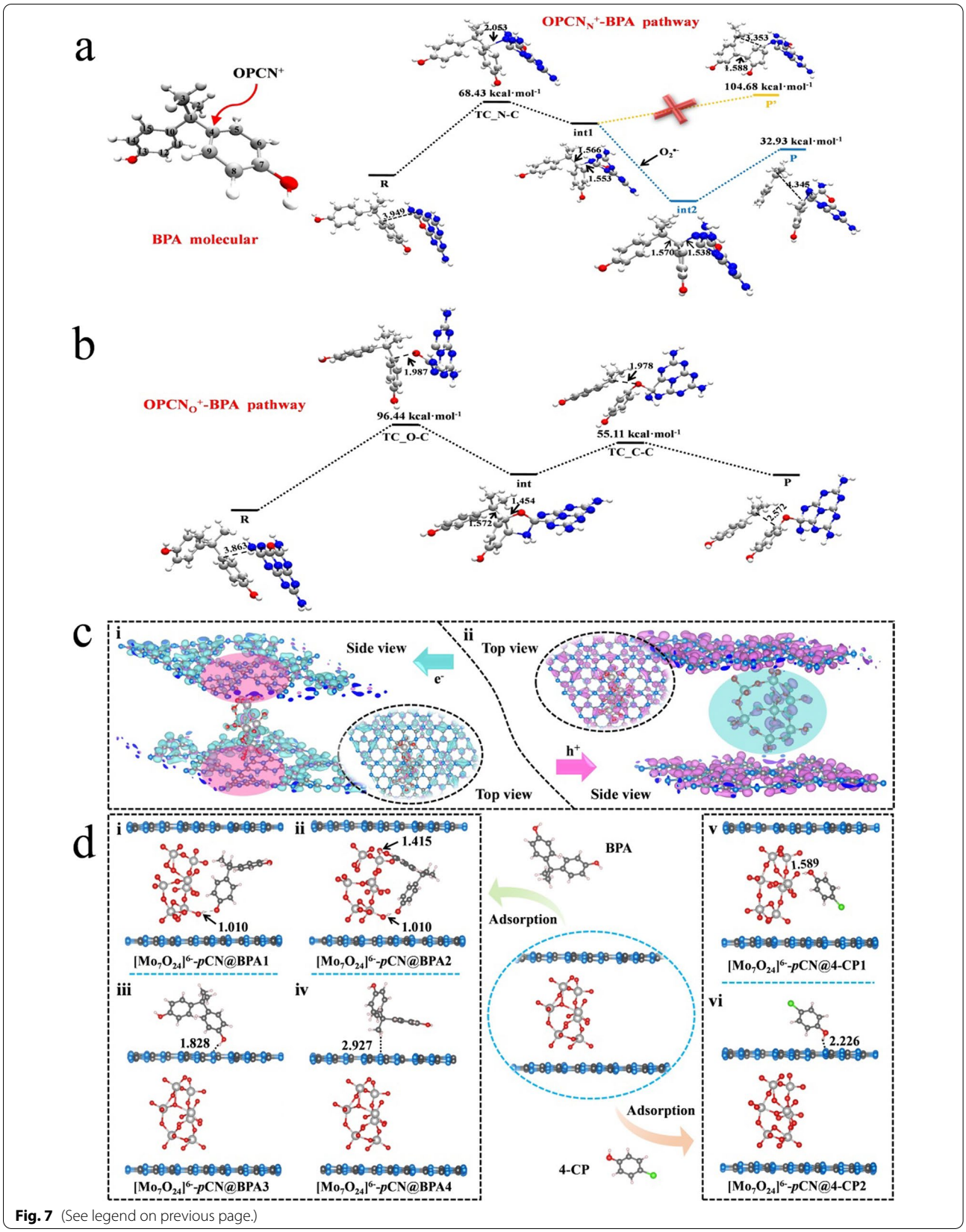

Fig. 7 (See legend on previous page.)

toxic to environmental ecosystem. The stability of the catalyst should be evaluated, especially for long aging time in complicated systems; (5) The final products should be analyzed exactly, especially the toxicity of the products; (6) the photocatalytic reduction of other redox-active metal ions and direct measurement of remobilization of re-oxidation of metal ions adsorbed on biochar should be studied, especially for long-term conditions. The biochar itself is an environmentally friendly material, which can improve the soil nutrients and decontaminate the soil pollution. With the development of technology, the real application of biochar and biochar-based materials in environmental pollution will attract extensively attention.

Acknowledgements
The authors thank the valuable comments of anonymous reviewers and Editor.

Author contributions
YL: Investigation, writing-original draft and editing; SZ: Investigation, writing-original draft; YC: Investigation, writing-original draft; LZ: Investigation; BH: Investigation, review and editing; SW: Review and editing; JC: Review and editing; XW: Investigation, writing—review and editing. All authors read and approved the final manuscript.

Funding
This work was supported by National Key Research and Development Program of China (2017YFA0207002), the National Natural Science Foundation of China (U2067215), the Key Research and Development Plan of Zhejiang Province (2021C03176) and Beijing Outstanding Young Scientist Program.

Availability of data and materials
Authors can confirm that all relevant data are included in the article.

Declarations

Ethical approval and consent to participate
Not applicable.

Consent for publication
Agree.

Competing interests
Xiangke Wang is an Associate editor of Biochar and was not involved in the editorial review, or the decision to publish this article. All authors declare that there are no competing interests in this manuscript.

Author details
[1]Key Laboratory of Pollution Exposure and Health Intervention of Zhejiang Province, College of Biological and Environment Engineering, Zhejiang Shuren University, Hangzhou 310015, People's Republic of China. [2]School of Life Science, Shaoxing University, Shaoxing 312000, People's Republic of China. [3]College of Environmental Science and Technology, North China Electric Power University, Beijing 102206, People's Republic of China. [4]School of Environmental Science and Engineering, Guangdong University of Petrochemical Technology, Maoming 525000, People's Republic of China. [5]College of Geography and Environmental Science, Zhejiang Normal University, Jinhua 321004, People's Republic of China.

Received: 12 May 2022 Accepted: 17 July 2022
Published online: 26 July 2022

References

Alam MS, Gorman-Lewis D, Chen N, Safari S, Baek K, Konhauser KO, Alessi DS (2018) Mechanisms of the removal of U(VI) from aqueous solution using biochar: a combined spectroscopic and modeling approach. Environ Sci Technol 52:13057–13067

Azalok KA, Oladipo AA, Gazi M (2021) UV-light-induced photocatalytic performance of reusable MnFe-LDO–biochar for tetracycline removal in water. J Photochem Photobiol a: Chem 405:112976

Baig SA, Zhu J, Muhammad N, Sheng TT, Xu XH (2014) Effect of synthesis methods on magnetic Kans grass biochar for enhanced As(III, V) adsorption from aqueous solutions. Biomass Bioenergy 71:299–310

Cai X, Li J, Liu Y, Yan Z, Tan X, Liu S, Zeng G, Gu Y, Hu X, Jiang L (2018) Titanium dioxide-coated biochar composites as adsorptive and photocatalytic degradation materials for the removal of aqueous organic pollutants. J Chem Technol Biotechnol 93:783–791

Cai Y, Liang Q, Yi Y, Chen Z, Yang H, Hu B, Liang L, Wang X (2022a) Application of covalent organic frameworks in environmental pollution management. Appl Catal A General 643:118733

Cai Y, Zhang Y, Lv Z, Zhang S, Gao F, Fang M, Kong M, Liu P, Tan X, Hu B, Wang X (2022b) Highly efficient uranium extraction by a piezo catalytic reduction-oxidation process. Appl Catal B: Environ 310:121343

Cao TT, Cui H, Zhang QW, Cui CW (2021) Facile synthesis of Co(II)-BiOCl@biochar nanosheets for photocatalytic degradation of p-nitrophenol under vacuum ultraviolet (VUV) irradiation. Appl Surf Sci 559:149938

Chandra S, Jagdale P, Medha I, Tiwari AK, Bartoli M, Nino AD, Olivito F (2021) Biochar-supported TiO_2-based nanocomposites for the photocatalytic degradation of sulfamethoxazole in water-a review. Toxic 9:313

Chen S, Lu W, Han J, Zhong H, Xu T, Wang G, Chen W (2019a) Robust three-dimensional g-C_3N_4@cellulose aerogel enhanced by cross-linked polyester fibers for simultaneous removal of hexavalent chromium and antibiotics. Chem Eng J 359:119–129

Chen M, Dai Y, Guo J, Yang H, Liu D, Zhai Y (2019b) Solvothermal synthesis of biochar@$ZnFe_2O_4$/BiOBr Z-scheme heterojunction for efficient photocatalytic ciprofloxacin degradation under visible light. Appl Surf Sci 493:1361–1367

Chen G, Wang H, Han L, Yang N, Hu B, Qiu M, Zhong X (2021a) Highly efficient removal of U(VI) by a novel biochar supported with FeS nanoparticles and chitosan composites. J Mol Liq 327:114807

Chen C, Shen Z, Qiu M (2021b) Enhanced U(VI) elimination from aqueous solution by FeS@biochar composites. Desalination Water Treat 210:393–401

Chen Z, He X, Li Q, Yang H, Liu Y, Wa L, Liu Z, Hu B, Wang X (2022a) Low-temperature plasma induced phosphate groups onto coffee residue-derived porous carbon for efficient U(VI) extraction. J Environ Sci 122:1–13

Chen T, Yu K, Dong C, Yuan X, Gong X, Lian J, Cao X, Li M, Zhou L, Hu B, He R, Zhu W, Wang X (2022b) Advanced photocatalysts for uranium extraction: elaborate design and future perspectives. Coord Chem Rev 467:214615

Cheng G, Zhang A, Zhao Z, Chai Z, Hu B, Han B, Ai Y, Wang X (2021) Extremely stable amidoxime functionalized covalent organic frameworks for uranium extraction from seawater with high efficiency and selectivity. Sci Bull 66:1996–2001

Cho DW, Yoon K, Kwon EE, Biswas JK, Song H (2017) Fabrication of magnetic biochar as a treatment medium for As(V) via pyrolysis of $FeCl_3$-pretreated spent coffee ground. Environ Poll 229:942–949

Dong XL, Ma LQ, Gress J, Harris W, Li YC (2014) Enhanced Cr(VI) reduction and As(III) oxidation in ice phase: important role of dissolved organic matter from biochar. J Hazard Mater 267:62–70

Fan J, Chen X, Xu ZB, Xu XY, Zhao L, Qiu H, Cao XD (2020) One-pot synthesis of nZVI-embedded biochar for remediation of two mining arsenic-contaminated soils: arsenic immobilization associated with iron transformation. J Hazard Mater 398:122901

Fang G, Liu C, Wang Y, Dionysiou DD, Zhou D (2017) Photogeneration of reactive oxygen species from biochar suspension for diethyl phthalate degradation. Appl Catal B Environ 214:34–45

Fang M, Tan X, Liu Z, Hu B, Wang X (2021) Recent progress on metal-enhanced photocatalysis: a review on the mechanism. Research 2021:9794329

Fazal T, Razzaq A, Javed F, Hafeez A, Rashid N, Amjad US, Rehman MSU, Faisal A, Rehman F (2020) Integrating adsorption and photocatalysis: a cost effective strategy for textile wastewater treatment using hybrid biochar-TiO_2 composite. J Hazard Mater 390:121623

Feng Z, Yuan R, Wang F, Chen Z, Zhou B, Chen H (2021) Preparation of magnetic biochar and its application in catalytic degradation of organic pollutants: a review. Sci Total Environ 765:142673

Gasim MF, Choong ZY, Koo PL, Low SC, Abdurahman MH, Ho YC, Mohamad M, Suryawan IWK, Lim JW, Oh WD (2022) Application of biochar as functional material for remediation of organic pollutants in water: an overview. Catalysts 12:210

Geng A, Xu L, Gan L, Mei C, Wang L, Fang X, Li M, Pan M, Han S, Cui J (2020) Using wood flour waste to produce biochar as the support to enhance the visible-light photocatalytic performance of BiOBr for organic and inorganic contaminants removal. Chemosphere 250:126291

Gholami P, Khataee A, Soltani RDC, Dinpazhoh L, Bhatnagar A (2020) Photocatalytic degradation of gemifloxacin antibiotic using Zn-Co-LDH@biochar nanocomposite. J Hazard Mater 382:121070

Goncalves MG, Veiga PAS, Fornari MR, Peralta-Zamora P, Mangrich AS, Silvestri S (2020) Relationship of the physicochemical properties of novel ZnO/biochar composites to their efficiencies in the degradation of sulfamethoxazole and methyl orange. Sci Total Environ 748:141381

Guo Y, Liu X, Xie S, Liu H, Wang C, Wang L (2022) 3D ZnO modified biochar-based hydrogels for removing U(VI) in aqueous solution. Colloid Surf A 642:128606

Hao M, Qiu M, Yang H, Hu B, Wang X (2021) Recent advances on preparation and environmental applications of MOF-derived carbons in catalysis. Sci Total Environ 760:143333

Hao M, Chen Z, Yang H, Waterhouse GIN, Ma S, Wang S (2022a) Pyridinium salt-based covalent organic framework with well-defined nanochannels for efficient and selective capture of aqueous $^{99}TcO_4^-$. Sci Bull 67:924–932

Hao M, Liu X, Liu X, Zhang J, Yang H, Waterhouse GIN, Wang X, Ma S (2022b) Converging cooperative functions into the nanospace of covalent organic frameworks for efficient uranium extraction from seawater. CCS Chem 4:2294–2307

Hu HS (2022) Preparation of N-doped TiO_2/biochar composite catalysts and its application for photoelectrochemical degradation of cephalosporin antibiotics. Int J Electrochem Sci 17:220330

Hu Q, Zhu Y, Hu B, Lu S, Sheng G (2018) Mechanistic insights into sequestration of U(VI) toward magnetic biochar: batch, XPS and EXAFS techniques. J Environ Sci 70:217–225

Hu B, Ai Y, Jin J, Hayat T, Alsaedi A, Zhuang L, Wang X (2020) Efficient elimination of organic and inorganic pollutants by biochar-based nanomaterials. Biochar 2:47–64

Huang Q, Song S, Chen Z, Hu B, Chen J, Wang X (2019) Biochar-based materials and their applications in removal of organic contaminants from wastewater: state-of-the-art review. Biochar 1:45–73

Huang W, Tang Y, Zhang X, Luo Z, Zhang J (2022) nZVI-biochar derived from Fe_3O_4-loaded rabbit manure for activation of peroxymonosulfate to degrade sulfamethoxazole. J Water Proc Eng 45:102470

Jeon P, Lee ME, Baek K (2017) Adsorption and photocatalytic activity of biochar with graphitic carbon nitride (g-C_3N_4). J Taiwan Inst Chem Eng 77:244–249

Kang F, Shi C, Li W, Eqi M, Liu Z, Zheng X, Huang Z (2022) Honeycomb like CdS/sulphur-modified biochar composites with enhanced adsorption-photocatalytic capacity for effective removal of rhodamine B. J Environ Chem Eng 10:106942

Karpuraranjith M, Chen Y, Ramadoss M, Wang B, Yang H, Rajaboopathi S, Yang D (2021) Magnetically recyclable magnetic biochar graphitic carbon nitride nanoarchitectures for highly efficient charge separation and stable photocatalytic activity under visible-light irradiation. J Molecule Liquid 326:115315

Khataee A, Kalderis D, Gholami P, Fazli A, Moschogiannaki M, Binas V, Lykaki M, Konsolskis M (2019) Cu_2O-CuO@biochar composite: synthesis, characterization and its efficient photocatalytic performance. Appl Surf Sci 498:143846

Kim JR, Kan E (2016) Heterogeneous photocatalytic degradation of sulfamethoxazole in water using a biochar-supported TiO_2 photocatalyst. J Environ Manag 180:94–101

Kumar A, Kumar A, Sharma G, Naushad M, Stadler FJ, Ghfar AA, Dhiman P, Saini RV (2017) Sustainable nano-hybrids of magnetic biochar supported g-C_3N_4/$FeVO_4$ for solar powered degradation of noxious pollutants-Synergism of adsorption, photocatalysis & photo-ozonation. J Clean Prod 165:431–451

Kumari N, Chhabra T, Kumar A, Krishnan V (2021) Bioderived carbon supported bismuth molybdate nanocomposites as bifunctional catalysts for removal of organic pollutants: adsorption and photocatalytic studies. Mater Lett 302:130455

Li C, Zhang L, Gao Y, Li A (2018) Facile synthesis of nano ZnO/ZnS modified biochar by directly pyrolyzing of zinc contaminated corn stover for Pb(II), Cu(II) and Cr(VI) removal. Waste Manage 79:625–637

Li K, Huang Z, Zhu S, Luo S, Yan L, Dai Y, Guo Y, Yang Y (2019a) Removal of Cr(VI) from water by a biochar-coupled g-C_3N_4 nanosheets composite and performance of a recycled photocatalyst in single and combined pollution systems. Appl Catal B Environ 243:386–396

Li X, Qian X, An X, Huang J (2019b) Preparation of a novel composite comprising biochar skeleton and "chrysanthemum" g-C_3N_4 for enhanced visible light photocatalytic degradation of formaldehyde. Appl Surf Sci 487:1262–1270

Li X, Wang C, Zhang J, Liu LJ, B, Chen G, (2020) Preparation and application of magnetic biochar in water treatment: a critical review. Sci Total Environ 711:134847

Li Q, Chen Z, Wang H, Yang H, Wen T, Wang S, Hu B, Wang X (2021a) Removal of organic compounds by nanoscale zero-valent iron and its composites. Sci Total Environ 792:148546

Li S, Hu Y, Shen Z, Cai Y, Ji Z, Tan X, Liu Z, Zhao G, Hu S, Wang X (2021b) Rapid and selective uranium extraction from aqueous solution under visible light in the absence of solid photocatalyst. Sci China Chem 64:1323–1331

Liang S, Shi S, Zhang H, Qiu J, Yu W, Li M, Gan Q, Yu W, Xiao K, Liu B, Hu J, Hou H, Yang J (2019) One-pot solvothermal synthesis of magnetic biochar from waste biomass: formation mechanism and efficient adsorption of Cr(VI) in an aqueous solution. Sci Total Environ 695:133886

Liang L, Xi F, Tan W, Meng X, Hu B, Wang X (2021) Review of organic pollutants and heavy metals removal by biochar and biochar-based composites. Biochar 3:255–281

Liu C, Hsu PC, Xie J, Zhao J, Wu T, Wang H, Liu W, Zhang J, Chu S, Cui Y (2017) A half-wave rectified alternating current electrochemical method for uranium extraction from seawater. Nat Energy 2:17007

Liu X, Pang H, Liu X, Li Q, Zhang N, Mao L, Qiu M, Hu B, Yang H, Wang X (2021a) Orderly porous covalent organic frameworks-based materials: superior adsorbents for pollutants removal from aqueous solutions. Innovation 2:100076

Liu X, Ma R, Zhuang L, Hu B, Chen J, Liu X, Wang X (2021b) Recent developments of doped g-C_3N_4 photocatalysts for the degradation of organic pollutants. Critical Rev Environ Sci Technol 51:751–790

Liu RR, Wang H, Han L, Hu BW, Qiu MQ (2021c) Reductive and adsorptive elimination of U(VI) ions in aqueous solution by SFeS@biochar composites. Environ Sci Poll Res 28:55176–55185

Liu XL, Verma G, Chen ZS, Hu BW, Huang QF, Yang H, Ma SQ, Wang XK (2022a) Metal-organic framework nanocrystals derived hollow porous materials: synthetic strategies and emerging applications. Innovation 3:100281

Liu X, Xie Y, Hao M, Chen Z, Yang H, Waterhouse GIN, Ma S, Wang X (2022b) Highly efficient electrocatalytic uranium extraction from seawater over an amidoxime—functionalized In—N—C catalyst. Adv Sci 9:2201735

Lu L, Shan R, Shi Y, Wang S, Yuan H (2019) A novel TiO_2/biochar composite catalysts for photocatalytic degradation of methyl orange. Chemosphere 222:391–398

Lu L, Yu W, Wang Y, Zhang K, Zhu X, Zhang Y, Wu Y, Ullah H, Xiao X, Chen B (2020) Application of biochar-based materials in environmental remediation: from multi-level structures to specific devices. Biochar 2:1–31

Mandal S, Sarkar B, Bolan N, Ok YS, Naidu R (2017) Enhancement of chromate reduction in soils by surface modified biochar. J Environ Manag 186:277–284

Mao W, Zhang L, Liu Y, Wang T, Bai Y, Guan Y (2021) Facile assembled N, S-codoped corn straw biochar loaded Bi_2WO_6 with the enhanced electron-rich feature for the efficient photocatalytic removal of ciprofloxacin and Cr(VI). Chemosphere 263:127988

Minh TD, Song J, Deb A, Cha L, Srivastava V, Sillanpaa M (2020) Biochar based catalysts for the abatement of emerging pollutants: a review. Chem Eng J 394:124856

Navarathna CM, Dewage NB, Karunanayake AG, Farmer EL, Perez F, Hassan EB, Mlsna TE, Pittman CU (2020) Rhodamine B adsorptive removal and photocatalytic degradation on MIL-53-Fe MOF/magnetic magnetite/biochar composites. J Inorg Organometal Mater 30:214–229

Ndoun MC, Elliott HA, Preisendanz HE, Williams CF, Knopf A, Watson JE (2021) Adsorption of pharmaceuticals from aqueous solutions using biochar derived from cotton gin waste and guayule bagasse. Biochar 3:89–104

Ouyang D, Chen Y, Yan J, Qian L, Han L, Chen M (2019) Activation mechanism of peroxymonosulfate by biochar for catalytic degradation of 1,4-dioxane: Important role of biochar defect structures. Chem Eng J 370:614–624

Pang HW, Diao ZF, Wang XX, Ma Y, Yu SJ, Zhu HT, Chen ZS, Hu BW, Chen JR, Wang XK (2019) Adsorptive and reductive removal of U(VI) by dictyophora indusiate-derived biochar supported sulfide NZVI from wastewater. Chem Eng J 366:368–377

Peng H, Li Y, Wen J, Zheng X (2021) Synthesis of $ZnFe_2O_4$/B, N-codoped biochar via microwave-assisted pyrolysis for enhancing adsorption-photocatalytic elimination of tetracycline hydrochloride. Ind Crop Prod 172:114066

Pi L, Jiang R, Zhou W, Zhu H, Xiao W, Wang D, Mao X (2015) g-C_3N_4 Modified biochar as an adsorptive and photocatalytic material for decontamination of aqueous organic pollutants. Appl Surf Sci 358:231–239

Pointurier F, Marie O (2013) Use of micro-Raman spectrometry coupled with scanning electron microscopy to determine the chemical form of uraniu compounds in micrometer-size particles. J Raman Spectrosc 44:1753–1759

Qiu M, Hu B, Chen Z, Yang H, Zhuang L, Wang X (2021) Challenges of organic pollutant photocatalysis by biochar-based catalysts. Biochar 3:117–123

Qiu M, Liu L, Ling Q, Cai Y, Yu S, Wang S, Fu D, Hu B, Wang X (2022) Biochar for the removal of contaminants from soil and water: a review. Biochar 4:19

Rajapaksha AU, Alam MS, Chen N, Alessi DS, Igalavithana AD, Tsang DCW, Ok YS (2018) Removal of hexavalent chromium in aqueous solutions using biochar: chemical and spectroscopic investigations. Sci Total Environ 625:1567–1573

Siara S, Elvis C, Harishkumar R, Chellam PV (2022) $ZnAl_2O_4$ supported on lychee-biochar applied to ibuprofen photodegradation. Mater Res Bull 145:111530

Silvestri S, Stefanello N, Sulkovski AA, Foletto EL (2020) Preparation of TiO_2 supported on MDF biochar for simultaneous removal of methylene blue by adsorption and photocatalysis. J Chem Technol Biotechnol 95:2723–2729

Stefaniak EA, Alsecz A, Sajó IE, Worobiec A, Máthé Z, Török S, Grieken RV (2008) Recognition of uranium oxides in soil particulate matter by means of μ-Raman spectrometry. J Nucl Mater 381:278–283

Sun Z, Zhao L, Liu C, Zhen Y, Ma J (2019) Catalytic ozonation of ketoprofen with in situ N-doped carbon: a novel synergetic mechanism of hydroxyl radical oxidation and an intra-electron-transfer nonradical reaction. Environ Sci Technol 53:10342–10351

Sutar S, Patil P, Jadhav J (2022) Recent advances in biochar technology for textile dyes wastewater remediation: a review. Environ Res 209:112841

Talukdar K, Jun BM, Yoon Y, Fayyza A, Park CM (2020) Novel Z-scheme Ag_3PO_4/Fe_3O_4-activated biochar photocatalyst with enhanced visible-light catalytic performance toward degradation of bisphenol A. J Hazard Mater 398:123025

Tan G, Mao Y, Wang H, Junaid M, Xu N (2019) Comparison of biochar- and activated carbon-supported zerovalent iron for the removal of As(IV) and Se(VI): influence of pH, ionic strength and natural organic matter. Environ Sci Poll Res 26:21609–21618

Tho PT, Van HT, Nguyen LH, Hoang TK, Tran TNH, Nguyen TT, Nguyen TBH, Nguyen VQ, Sy HL, Thai VN, Tran QB, Sadeghzaden SM, Asadpour R, Thang PQ (2021) Enhanced simultaneous adsorption of As(III), Cd(II), Pb(II)and Cr(VI) ions from aqueous solution using cassava root husk-derived biochar loaded with ZnO nanoparticles. RSC Adv 11:18881–188897

Wang X, Chen L, Wang L, Fan Q, Pan D, Li J, Chi F, Yu S, Xie Y, Xiao C, Luo F, Wang J, Wang X, Chen C, Wu W, Shi W, Wang S, Wang X (2019a) Synthesis of novel nanomaterials and their application in efficient removal of radionuclides. Sci China Chem 62:933–967

Wang T, Liu X, Men Q, Ma C, Liu Y, Ma W, Liu Z, Wei M, Li C, Yan Y (2019b) Surface plasmon resonance effect of Ag nanoparticles for improving the photocatalytic performance of biochar quantum-dot/$Bi_4Ti_3O_{12}$ nanosheets. Chinese J Catalysis 40:886–894

Wang T, Liu S, Mao W, Bai Y, Chiang K, Shah K, Pza-Ferreiro J (2020) Novel Bi_2WO_6 loaded N-biochar composites with enhanced photocatalytic degradation of rhodamine B and Cr(VI). J Hazard Mater 389:121827

Wang L, Lu Z, Wei X, Fang M, Wang X (2021) Application of improved grey model in photocatalytic data prediction. J Inorg Mater 36:871–876

Wang S, Shi L, Yu S, Pang H, Qiu M, Song G, Fu D, Hu B, Wang X (2022) Effect of shewanella oneidensis MR-1 on U(VI) sequestration by montmorillonite. J Environ Radioact 242:106798

Wei X, Yu F, Ji J, Cai Y, Zou W, Zheng Y, Huang J, Zhang Y, Yang Y, Naushad M, Gao B, Dong L (2021) Porous biochar supported Ag_3PO_4 photocatalyst for "two-in-one" synergistic adsorptive-photocatalytic removal of methylene blue under visible light irradiation. J Environ Chem Eng 9:106753

Welter N, Leichtweis J, Silvestri S, Sanchez PIZ, Mejia ACC, Carissimi E (2022) Preparation of a new green composite based on chitin biochar and $ZnFe_2O_4$ for photo-Fenton degradation of Rhodamine B. J Hazard Mater 901:163758

Xia D, Tan F, Zhang C, Jing X, Chen Z, Li H, Zheng Y, Li Q, Wang Y (2016) ZnCl2-activated biochar from biogas residue facilitates aqueous As(III) removal. Appl Surf Sci 377:361–369

Xiao R, Wang JJ, Li R, Park J, Meng Y, Zhou B, Pensky S, Zhang Z (2018) Enhanced sorption of hexavalent chromium [Cr(VI)] from aqueous solutions by diluted sulfuric acid-assisted MgO-coated biochar composite. Chemosphere 208:408–416

Xiao Y, Lyu H, Tang J, Wang K, Sun H (2020) Effects of ball milling on the photochemistry of biochar: enrofloxacin degradation and possible mechanisms. Chem Eng J 384:123311

Xiao Y, Lyu H, Yang C, Zhao B, Wang L, Tang J (2021) Graphitic carbon nitride/biochar composite synthesized by a facile ball-milling method for the adsorption and photocatalytic degradation of enrofloxacin. J Environ Sci 103:93–107

Yan LL, Kong L, Qu Z, Li L, Shen GQ (2015) Magnetic biochar decorated with ZnS nanocrytals for Pb(II) removal. ACS Sustain Chem Eng 3:125–132

Yang H, Liu X, Hao M, Xie Y, Wang X, Tian H, Waterhouse GIN, Kruge PE, Telfer SG, Ma S (2021a) Functionalized iron—nitrogen—carbon electrocatalyst provides a reversible electron transfer platform for efficient uranium extraction from seawater. Adv Mater 33:2106621

Yang CX, Zhu Q, Dong WP, Fan YQ, Wang WL (2021b) Preparation and characterization of phosphoric acid-modified biochar nanomaterials with highly efficient adsorption and photodegradation ability. Langmuir 37:9253–9263

Yang J, Zhu W, Yao Q, Lu G, Yang C, Dang Z (2021c) Photochemical reactivity of nitrogen-doped biochars under simulated sunlight irradiation: generation of singlet oxygen. J Hazard Mater 410:124547

Yao L, Yang H, Chen Z, Qiu M, Hu B, Wang X (2021) Bismuth oxychloride-based materials for the removal of organic pollutants in wastewater. Chemosphere 273:128576

Ye S, Yan M, Tan X, Liang J, Zeng G, Wu H, Song B, Zhou C, Yang Y, Wang H (2019) Facile assembled biochar-based nanocomposite with improved graphitization for efficient photocatalytic activity driven by visible light. Appl Catal B Environ 250:78–88

Yu J, Jiang C, Guan Q, Ning P, Gu J, Chen Q, Zhang J, Miao R (2018) Enhanced removal of Cr(VI) from aqueous solution by supported ZnO nanoparticles on biochar derived from waste water hyacinth. Chemosphere 195:632–640

Yu Y, An Q, Jin L, Luo N, Li Z, Jiang J (2020) Unraveling sorption of Cr (VI) from aqueous solution by FeCl3 and ZnCl2- modified corn stalks biochar: implicit mechanism and application. Biores Technol 297:122466

Yu S, Pang H, Huang S, Tang H, Wang S, Qiu M, Chen Z, Yang H, Song G, Fu D, Hu B, Wang X (2021a) Recent advances in metal-organic frameworks membranes for water treatment: a review. Sci Total Environ 800:149662

Yu F, Tian F, Zou H, Ye Z, Peng C, Huang J, Zheng Y, Zhang Y, Yang Y, Wei X, Gao B (2021b) ZnO/biochar nanocomposites via solvent free ball milling for enhanced adsorption and photocatalytic degradation of methylene blue. J Hazard Mater 415:125511

Yu S, Tang H, Zhang D, Wang S, Qiu M, Song G, Fu D, Hu B, Wang X (2022) MXenes as emerging nanomaterials in water purification and environmental remediation. Sci Total Environ 811:152280

Zhai Y, Dai Y, Guo J, Zhou L, Chen M, Yang H, Peng L (2020) Novel biochar@$CoFe_2O_4$/Ag_3PO_4 photocatalysts for highly efficient degradation

of bisphenol a under visible-light irradiation. J Colloid Interface Sci 560:111–121
Zhang H, Wang Z, Li R, Guo J, Li Y, Zhu J, Xie X (2017) TiO_2 supported on reed straw biochar as an adsorptive and photocatalytic composite for the efficient degradation of sulfamethoxazole in aqueous matrices. Chemosphere 185:351–360
Zhang X, Fu W, Yin Y, Chen Z, Qiu R, Simonnot MO, Wang X (2018a) Adsorption-reduction removal of Cr(VI) by tobacco petiole pyrolytic biochar: batch experiment, kinetic and mechanism studies. Biores Technol 268:149–157
Zhang X, Lv L, Qin Y, Xu M, Jia X, Chen Z (2018b) Removal of aqueous Cr(VI) by a magnetic biochar derived from Melia azedarach wood. Biores Technol 256:1–10
Zhang S, Liu Y, Gu PC, Ma R, Wen T, Zhao GX, Li L, Ai YJ, Hu C, Wang XK (2019a) Enhanced photodegradation of toxic organic pollutants using dual-oxygen-doped porous g-C_3N_4: mechanism exploration from both experimental and DFT studies. Appl Catal B Environ 248:1–10
Zhang S, Song S, Gu P, Ma R, Wei DL, Zhao GX, Wen T, Jehan R, Hu BW, Wang XK (2019b) Visible-light-driven activation of persulfate over cyano and hydroxyl group co-modified mesoporous g-C_3N_4 for boosting bisphenol A degradation. J Mater Chem A 7:5552–5560
Zhang P, Min L, Tang J, Rafiq MK, Sun H (2020) Sorption and degradation of imidacloprid and clothianidin in Chinese paddy soil and red soil amended with biochars. Biochar 2:329–341
Zhang S, Wang JQ, Zhang Y, Ma JZ, Huang LTY, Yu SJ, Chen L, Song G, Qiu MQ, Wang XX (2021a) Applications of water-stable metal-organic frameworks in the removal of water pollutants: a review. Environ Poll 291:118076
Zhang Z, Wang G, Li W, Zhang L, Guo B, Ding L, Li X (2021b) Photocatalytic activity of magnetic nano-β-FeOOH/Fe_3O_4/biochar composites for the enhanced degradation of methyl orange under visible light. Nanomaterials 11:526
Zhang Y, Liu H, Gao F, Tan X, Cai Y, Hu B, Huang Q, Fang M, Wang X (2022a) Application of MOFs and COFs for photocatalysis in CO_2 reduction, H_2 generation, and environmental treatment. EnergyChem 4:100078
Zhang S, Liu Y, Ma R, Jia D, Wen T, Ai Y, Zhao G, Fang F, Hu B, Wang X (2022b) Molybdenum (VI)-oxo clusters incorporation activates g-C_3N_4 with simultaneously regulating charge transfer and reaction centers for boosting photocatalytic performance. Adv Funct Mater 32:2204175
Zhao N, Yin Z, Liu F, Zhang M, Lv Y, Hao Z, Pan G, Zhang J (2018) Environmentally persistent free radicals mediated removal of Cr(VI) from highly saline water by corn straw biochars. Biores Technol 260:294–301
Zhao C, Wang B, Theng BKG, Wu P, Liu F, Wang S, Lee X, Chen M, Li L, Zhang X (2021) Formation and mechanisms of nano-metal oxide-biochar composites for pollutants removal: a review. Sci Total Environ 767:145305
Zheng Y, Yang Y, Zou W, Luo Y, Dong L, Gao B (2019) Facile one-step synthesis of graphitic carbon nitride-modified biochar for the removal of reactive red 120 through adsorption and photocatalytic degradation. Biochar 1:89–96
Zheng C, Yang Z, Si M, Zhu F, Yang W, Zhao F, Shi Y (2021) Application of biochars in the remediation of chromium contamination: Fabrication, mechanisms, and interfering species. J Hazard Mater 407:124376
Zou Y, Hu Y, Shen Z, Yao L, Tang D, Zhang S, Wang S, Hu B, Zhao G, Wang X (2022) Application of aluminosilicate clay mineral-based composites in photocatalysis. J Environ Sci 115:190–214